Mechanics of Materials 41 (2009) 599–621

Contents lists available at ScienceDirect

Mechanics of Materials

journal homepage: www.elsevier.com/locate/mechmat

Modelling of thermo-viscoplastic behaviour of *DH-36* and *Weldox 460-E* structural steels at wide ranges of strain rates and temperatures, comparison of constitutive relations for impact problems

J.R. Klepaczko [a], A. Rusinek [b], J.A. Rodríguez-Martínez [c,*], R.B. Pęcherski [d], A. Arias [c]

[a] *Laboratory of Physics and Mechanics of Materials, UMR CNRS 7554, Paul Verlaine University of Metz, Ile du Saulcy, 57045 Metz, France*
[b] *National Engineering School of Metz (ENIM), Laboratory of Mechanical Reliability (LFM), Ile du Saulcy, 57000 Metz, France*
[c] *Department of Continuum Mechanics and Structural Analysis, University Carlos III of Madrid, Avda. de la Universidad 30, 28911 Leganés, Madrid, Spain*
[d] *IPPT – Institute of Fundamental Technological Research, Polish Academy of Sciences, ul. Swietokrzyka 21, 00-049 Warsaw, Poland*

ARTICLE INFO

Article history:
Received 30 March 2008
Received in revised form 1 September 2008

This paper is dedicated to our friend, Prof. Janusz Roman Klepaczko who passed away in August 15, 2008, for his pioneer contribution in the area of dynamic behaviour of materials.

ABSTRACT

In this paper, the thermo-viscoplastic behaviour of *DH-36* and *Weldox-460-E* steels is analyzed at wide ranges of strain rates and temperatures. These materials are commonly used for naval applications. Thus, they may be subjected to a wide range of exploitation temperatures and at the same time to high strain rates due to accidental impact or explosion. The thermo-viscoplastic behaviour of these materials has been modeled by application of *RK (Rusinek–Klepaczko)* constitutive relation. The predictions obtained using *RK* constitutive relation have been compared with *JC* (*Johnson–Cook*) and *PB* (*Physical Base*) constitutive relations with use of the experimental results reported in the works of Nemat-Nasser and Guo [Nemat-Nasser, S., Guo, W.G., 2003. Thermomechanical response of *DH-36* structural steel over a wide range of strain rates and temperatures. Mech. Mat. 35, 1023–1047] and Borvik et al. [Børvik, T., Hopperstad, O.S., Berstad, T., Langseth, M., 2001. A computational model of viscoplasticity and ductile damage for impact and penetration. Eur. J. Solid. Mech. A. 20, 685–712]. For both metals, a satisfactory agreement is reported between the experimental results and the analytical predictions using *RK* model at wide ranges of strain rates and temperatures (10^{-3} s^{-1} to 10^{4} s^{-1}, and 77 K to about 1000 K). Especially for high strain rate level, the predictions of *RK* model are notably more precise than those predictions obtained using *PB* and *JC* models. This proof converts *RK* model in suitable for modeling impact problems. Finally, numerical simulations of perforation process of *DH-36* and *Weldox 460-E* steel plates impacted by conical non-deformable projectiles have been carried out using *RK* and *JC* models. Numerical results using FE simulations have revealed substantial influence of the constitutive relation concerning the ballistic limit, residual velocity and failure time predictions for the same initial and boundary conditions.

1. Introduction

The study of materials subjected to extreme loading conditions as for example crash, impact or explosion, and extreme environmental conditions, as for example low and high temperatures, presents a considerable interest in different application fields as for example in naval engineering. Nowadays several publications can be found in the international literature dealing with high strain rate behaviour of different metallic materials directly related to engineering applications like automotive (Rusinek et al., 2008a; Larour et al., 2007; Mae et al., 2007; Smerd et al., 2005), civil (Kobayashi et al., 2008; Shanmugama et al., in press; Zaera et al., 2002), aeronautical (Fasanella and Jackson, 2001; Piekutowski, 1999) or naval (Nemat-Nasser and Guo, 2003; Martineau et al., 2004) industries. Particularly, the behaviour of high-strength sheet metals

* Corresponding author. Tel.: +34 91 624 8460; fax: +34 91 624 9430.
E-mail address: jarmarti@ing.uc3m.es (J.A. Rodríguez-Martínez).

0167-6636/$ - see front matter © 2008 Elsevier Ltd. All rights reserved.
doi:10.1016/j.mechmat.2008.11.004

when subjected to high velocity impact by rigid projectiles has raised a considerable interest as it is illustrated in the works (Borvik et al., 2002a,b; Gupta et al., 2006, 2007; Arias et al., 2008; Rusinek et al., 2008b). A common characteristic of most of those works is that during experiment of perforation, specimen remains at room temperature during a high strain rate deformation. However, this circumstance is not consistent with the service conditions of many structures, which are frequently subjected to a wide range of initial temperatures in addition to high strain rate levels.

In order to model the thermo-viscoplastic behaviour of metallic materials under the mentioned above loading conditions, several constitutive relations can be found in the literature, (Cowper and Symonds, 1952; Bodner and Partom, 1975; Steinberg et al., 1980; Nemat-Nasser, 1982; Johnson and Cook, 1983; Zerilli and Armstrong, 1987; Khan, 1998; Rusinek and Klepaczko, 2001; Durrenberger et al., 2007; Voyiadjis and Almasri, 2008). The phenomenological approaches as that due to Johnson and Cook (*JC*) (Johnson and Cook, 1983) are widely used, mainly because of the reduced number of material constants necessary for calibration and the simplicity in applications. More physical approaches are reported in Bodner and Partom (1975); Zerilli and Armstrong (1987); Durrenberger et al. (2007); Voyiadjis and Almasri (2008). They are more complex to calibrate and less used in engineering practice. A critical analysis dealing with this topic can be also found in the works of Liang and Khan (1999) and Rusinek et al. (2007a).

The relevance of providing a good material definition for *DH-36* and *Weldox 460-E* steels within a wide range of strain rates and temperatures comes from its application field. These steels are frequently used in naval applications as military boats, submarines, water towers or offshore structures, as reported for example in Nemat-Nasser and Guo (2003). Naval structures can be subjected to high strain rate level due to impact events induced by iceberg collision, rock falling or attack, but it also must be taken into account that these dynamic loading conditions can take place under a wide range of temperatures. For example, a submarine can be subjected to relatively high temperature due to sun exposition or to a low temperature in Polar Regions.

These remarks lead to conclusion that one must analyze diverse cases of loading combined with temperature within the interval $173 \leqslant T_0 \leqslant 373$ K and strain rates from quasi-static to dynamic conditions: $10^{-3}\ \mathrm{s}^{-1} \leq \dot{\bar{\varepsilon}}_p \leq 10^{5}\ \mathrm{s}^{-1}$. In the present case, a semi-physical model due to Rusinek and Klepaczko (2001) (*RK*) is used to model the behaviour of *DH-36* and *Weldox-460-E* steels. This constitutive relation has been previously used to define the thermo-viscoplastic behaviour of several steels frequently used in automotive industry (Larour et al., 2007) when subjected to different quasi-static and dynamic loading conditions such as tension and shear (Rusinek and Klepaczko, 2001; Rusinek et al., 2005), ring expansion (Rusinek et al., 2007b) or impact perforation (Rusinek et al., 2008c).

In this paper, a comparison is reported between different constitutive relations. In the case of *DH-36* steel the *RK*, *JC* and *PB* constitutive relations have been considered. In the case of *Weldox 460-E*, *RK* and *JC* constitutive relations are taken into account. The analysis has been carried out considering a wide range of strain rates and temperatures and the analytical predictions of the constitutive relations have been compared with experimental results reported in Nemat-Nasser and Guo (2003) and Børvik et al. (2001). It has been observed that the best agreement with experimental data is achieved by the analytical predictions obtained using *RK* constitutive relation.

In order to analyze the influence of constitutive relation when *DH-36* and *Weldox 460-E* steels are subjected to extreme loads, numerical simulations of perpendicular impact using conical non-deformable projectiles have been carried out. The numerical study was performed using the FE code ABAQUS/Explicit by application of 3D analysis. *RK* and *JC* constitutive relations were applied during the simulations assuming isotropic behaviour of the material.

In the case of *DH-36* steel, three different initial temperatures were assumed during simulations: ($T_{01} = 200$, $T_{02} = 296$, $T_{03} = 400$ K) with application of a wide range of impact velocities varying from $V_{bl} \leqslant V_0 \leqslant 400$ m/s, where V_{bl} is the ballistic limit velocity. In the case of *Weldox 460-E* steel the numerical results obtained have been compared with experimental data at room temperature reported in Borvik et al. (2002a) in the range of impact velocities mentioned above.

For both materials considered, relevant differences were found in the ballistic limit, the residual velocity and values of failure time predicted by *RK* and *JC* constitutive relations. Thus, it is noticed the influence of the material definition in the simulation of impact events.

2. Materials

The steels analyzed in this paper, *DH-36* and *Weldox 460-E*, consist of a ferrite–pearlitic (*BBC*) structure, where layers of pearlite lie between whole grains of ferrite. It is known that ferrite has lower strength and hardness, but higher plasticity and toughness, whereas pearlite has reversed properties.

The added elements as Ti, Mn, Al and Cr allow for carbon compatibility. These additive elements generate creation of carbide which increases the strength of steels. Concerning Cu it is allowing for reduction of transformation temperature $\alpha \rightarrow \gamma$ increasing the thinness of the pearlite and the hardness of this component. Concerning Mo it allows for increase of strength level at high temperature, such composition is frequently used for military applications or in nuclear reactors. The chemical element V is also used to obtain a high strength level at high temperature and to control the grain size growing (Rusinek, 2000).

2.1. DH-36 steel

DH-36 steel is a high strength structural steel used in naval constructions. The chemical composition of this material is given in Table 1 (Nemat-Nasser and Guo, 2003). This material is a high-strength low-alloy steel due to the carbon content which is relatively high: 0.14%.

Its average grain size is $D = 9$ μm. Although this material has a microstructure distribution different along the thickness due to the rolling process, the macroscopic behaviour $\bar{\sigma}(\bar{\varepsilon}_p, \dot{\bar{\varepsilon}}_p, T)$ is not affected. The same mechanical properties are found when the loading direction is perpendicular or parallel to the rolling direction. More details about the microstructure effect on the mechanical properties are given in Nemat-Nasser and Guo (2003) where an analysis of the thermo-viscoplastic behaviour of *DH-36* steel is reported in terms of different temperatures and strain rates. It has been observed during experiments that this material shows a strain aging phenomenon (Nemat-Nasser and Guo, 2003). It means an increase of the flow stress with temperature. This phenomenon is due to diffusion of carbon at specific temperature inducing a trapping of mobile dislocations by the Cottrell atmospheres. In that case an increase of the macroscopic stress level occurs. The temperature limits corresponding to manifestation of this phenomenon depend on the imposed strain rate, Fig. 1. A linear dependence of this effect (temperature of strain ageing) is observed with the logarithm of strain rate.

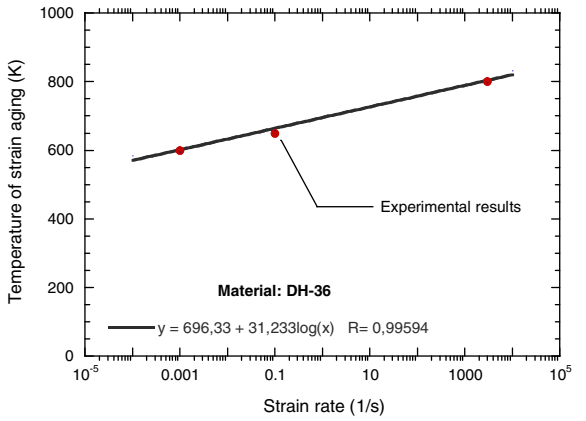

Fig. 1. Strain aging temperature vs. strain rate. Experimental results (Nemat-Nasser and Guo, 2003).

2.2. Weldox-46-E steel

Weldox is a group of high-strength steels that combines high strength with large ductility and good weldability. *Weldox 460 E* has particularly high yield stress, around $\sigma_y \approx 500$ MPa, with failure stress of $\sigma_{failure} \geqslant 1$ GPa, (Borvik et al., 1999; Børvik et al., 2001) .The high strength of *Weldox 460 E* is obtained by rolling process using a specific temperature, followed by a controlled cooling. The chemical composition of this steel is given in Table 2.

This steel is widely used for structural applications in several engineering fields, mainly in naval and civil constructions. Moreover, a substantial amount of studies concerning the dynamic behaviour of *Weldox 460 E* can be found in the international literature, mainly dealing with its behaviour during impact (Borvik et al., 1999, 2002a; Dey et al., 2004). The behaviour of the material can be assumed as isotropic (Børvik et al., 2001). Moreover, it shows a strain aging effect within the following temperature range, $400 < T_0 < 800$ K (Børvik et al., 2001).

3. Constitutive relations for steel alloys

In this section of the document the *RK*, *JC* and *PB* constitutive relations are analyzed. In the case of *RK* model, the procedure followed to obtain the material constants is outlined.

3.1. The Rusinek–Klepaczko (RK) model

This model (Rusinek and Klepaczko, 2001) was previously proven to approximate successfully the behaviour of several materials with BCC and FCC microstructures (Larour et al., 2007; Rusinek et al., 2005, 2007a,b, 2008c,d).

3.1.1. Description of the constitutive relation

This semi-physical model is based on an additive decomposition of the total stress, $\bar{\sigma}$. Thus, the total stress is an addition of two terms σ_μ and σ^*, which define respectively the strain hardening and thermal activation processes, Fig. 2. The first is called the internal stress and the second the effective stress.

Using this decomposition, the total stress is defined by Eq. (1). It is observed that the effective stress component σ^*, which defines the coupling strain rate-temperature, is independent of the level of plastic strain in comparison with the internal stress σ_μ which defines strain hardening. The first term defines the Young's modulus evolution with temperature, (Klepaczko, 1998), Eq. (2).

$$\bar{\sigma}(\bar{\varepsilon}_p, \dot{\bar{\varepsilon}}_p, T) = \frac{E(T)}{E_0}\left[\sigma_\mu(\bar{\varepsilon}_p, \dot{\bar{\varepsilon}}_p, T) + \sigma^*(\dot{\bar{\varepsilon}}_p, T)\right] \tag{1}$$

$$E(T) = E_0\left\{1 - \frac{T}{T_m}\exp\left[\theta^*\left(1 - \frac{T_m}{T}\right)\right]\right\} \tag{2}$$

where E_0, T_m and θ^* denote respectively the Young's modulus at $T = 0$, the melting temperature and the characteristic homologous temperature. In the case of ferritic steels $\theta \approx 0.5$ (Rusinek et al., 2008d).

The Young's modulus evolution with temperature is reported in the following figure, Fig. 3. This analytical formulation has been compared with experimental results corresponding to different ferritic steels. A good agreement is found concerning temperature sensitivity of Young's modulus.

The explicit formulation of the equivalent stress $\bar{\sigma}$ is given by Eq. (3). The internal stress is defined by the plasticity modulus B along with the rate and temperature

Table 1
Chemical composition of *DH-36* steel (Nemat-Nasser and Guo, 2003).

C	Mn	Cu	Si	Cr	Mo	V	Ti	Al	Nb	P	S
0.14	1.37	0.14	0.22	0.08	0.03	0.001	0.003	0.017	0.03	0.007	0.001

Table 2
Chemical composition of *Weldox-460-E* steel (Børvik et al., 2001).

C	Mn	Ni	Si	Cr	Mo	V	Ti	Al	Nb	P	S	B	N
0.08	1.40	0.04	0.26	0.02	0.007	0.04	0.01	0.032	0.028	0.008	0.002	0.00	0.006

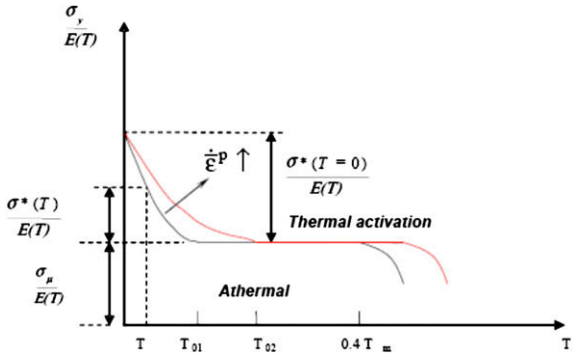

Fig. 2. Decomposition of the total stress by thermally activated part and the component related to strain hardening; the internal stress and the effective stress.

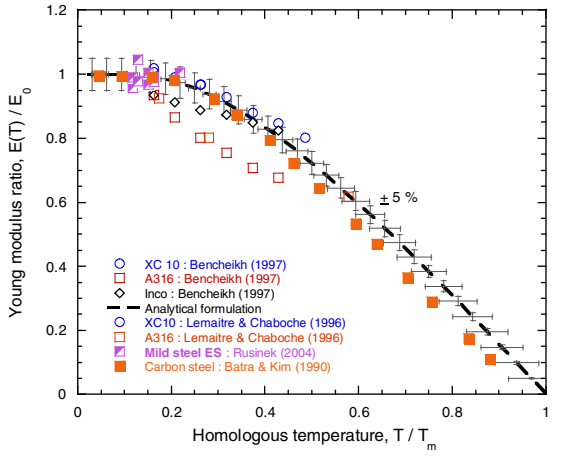

Fig. 3. Evolution of Young's modulus ratio of different steels with temperature.

dependent strain hardening exponent n. The effective stress is obtained using Arrhénius relation which couples temperature with strain rate. This kind of approach is well defined for thermal activation processes of plastic deformation.

$$\bar{\sigma}(\bar{\varepsilon}_p,\dot{\bar{\varepsilon}}_p,T)=\frac{E(T)}{E_0}\left[B(\dot{\bar{\varepsilon}}_p,T)(\varepsilon_0+\bar{\varepsilon}_p)^{n(\dot{\bar{\varepsilon}}_p,T)}+\sigma_0^*\left\langle 1-D_1\left(\frac{T}{T_m}\right)\log\left(\frac{\dot{\varepsilon}_{max}}{\dot{\bar{\varepsilon}}_p}\right)\right\rangle^{m^*}\right] \tag{3}$$

The modulus of plasticity B defines rate and temperature sensitivities of strain hardening, n is the strain hardening coefficient which is a specified function of strain rate and temperature, ε_0 is the strain level which defines the yield stress in quasi-static loading, σ_0^* is the effective stress at $T = 0$ K, D_1 is the material constant, $\dot{\varepsilon}^{max}$ is the maximum strain rate accepted for a particular analysis and m^* is the constant allowing to define the strain rate-temperature dependency (Klepaczko, 1987). The operator $\langle\bullet\rangle = \bullet$ if $\langle\bullet\rangle \geq 0$ or $\langle\bullet\rangle = 0$ if $\langle\bullet\rangle \leq 0$. Therefore the model eliminates the instantaneous rate sensitivity at low strain rates and high temperatures.

The explicit formulations describing the modulus of plasticity and strain hardening exponent with temperature and strain rate are given by, Eqs. (4) and (5).

$$B(\dot{\bar{\varepsilon}}_p,T)=B_0\left(\left(\frac{T}{T_m}\right)\log\left(\frac{\dot{\varepsilon}_{max}}{\dot{\bar{\varepsilon}}_p}\right)\right)^{-\nu} \tag{4}$$

$$n(\dot{\bar{\varepsilon}}_p,T)=n_0\left\langle 1-D_2\left(\frac{T}{T_m}\right)\log\frac{\dot{\bar{\varepsilon}}_p}{\dot{\varepsilon}_{min}}\right\rangle \tag{5}$$

where B_0 is the material constant, ν is the temperature sensitivity, n_0 is the strain hardening exponent at $T = 0$ K, D_2 is the material constant and $\dot{\varepsilon}^{min}$ is the minimum strain rate validated for this model. Therefore the limit of strain hardening is the ideal plasticity. A negative strain hardening is not accepted in the present case, $n \geqslant 0$.

In order to define the material constants of the model independently of the user, a specific methodology has been developed. This procedure is discussed in the next part of the paper.

3.1.2. Constant identification using RK model

The procedure to define the material constants was constructed allowing estimation, step by step of, all constants. Thus the material constants are determined automatically and independently of the user. It must be noticed that the constants are defined using physical assumptions. It is assumed that the model defines correctly the thermo-viscoplastic behaviour when the strain rate imposed varies from $\dot{\varepsilon}_{min} = 10^{-5}\ s^{-1}$ to $\dot{\varepsilon}_{max} = 10^{7}\ s^{-1}$. The first assumption is that at low strain rate $\dot{\bar{\varepsilon}}_p = 0.001\ s^{-1}$ the stress contribution due to thermal activation is reduced and in this case the following relation is imposed, Eq. (6). Under this assumption, it is possible to define the constant D_1 depending on the melting temperature T_m.

$$\begin{cases}\sigma^*(\dot{\bar{\varepsilon}}_p,T)\big|_{300\ K,0.001\ s^{-1}}=0\\ D_1=\left[\left(\frac{300}{T_m}\right)\log\left(\frac{\dot{\varepsilon}_{max}}{0.001}\right)\right]^{-1}\quad\text{is defined}\end{cases} \tag{6}$$

The contribution of the thermal activation to the total stress is zero at room temperature for quasi-static strain rate. Thus, the total stress level is defined by Eq. (7). Using this equation together with experimental results and applying the least squares method (Rusinek, 2000), the first estimation of B and n can be found.

$$\begin{cases}\bar{\sigma}(\bar{\varepsilon}_p,0.001,300)=\frac{E(300)}{E_0}\left[B(\varepsilon_0+\bar{\varepsilon}_p)^n+0\right]\\ B,n\ \text{first approximation for next fitting}\end{cases} \tag{7}$$

The second step assumes that the increase of the total stress $\bar{\sigma}$ with the strain rate, in comparison with the low strain rate defined as reference, $\dot{\bar{\varepsilon}}_p = 0.001\ s^{-1}$, is due to the effective stress σ^* which accounts for thermal activation processes. Thus, the stress increase is defined as follows, Eq. (8).

$$\begin{cases} \Delta\sigma|_{0.001\ s^{-1}\to\dot{\bar{\varepsilon}}_p}^{\bar{\varepsilon}_p} = \bar{\sigma}|_{\dot{\bar{\varepsilon}}_p}^{\bar{\varepsilon}_p} - \bar{\sigma}|_{0.001\ s^{-1}}^{\bar{\varepsilon}_p} = \sigma^*(\dot{\bar{\varepsilon}}_p, T)\big|^{\bar{\varepsilon}_p} \\ \sigma_0^*, m^* \quad \text{are} \quad \text{defined} \end{cases} \tag{8}$$

Using Eq. (8) together with experimental results for an imposed strain level, $\bar{\varepsilon}_p$, it is possible to determine the material constants m^* and σ_0^*. Generally, the strain level accounted for determination of the constants should be assumed not larger than 0.1, since adiabatic conditions at larger strain level induce a thermal softening of the material and in this case a decrease of the strain hardening rate. The limit of $\bar{\varepsilon}_p = 0.1$ allows for assuming isothermal condition in the material behaviour.

The third step is application of the complete equation for the total stress, Eq. (3), combined with experimental results, $\bar{\sigma} - \bar{\varepsilon}_p|_{\dot{\bar{\varepsilon}}_p}$. Therefore the stress dependency upon temperature and strain rate for the modulus of plasticity B and the strain hardening exponent n can be defined for an imposed strain rate. A first estimation to start the process of fitting is defined using Eq. (8). The next step is to approximate the trends of $B(\dot{\bar{\varepsilon}}_p, T)$ and $n(\dot{\bar{\varepsilon}}_p, T)$ using Eqs. (7) and (8).

The calibration method proposed is just limited to three tests performed at different strain rates. Required material data at low/intermediate strain rates ($\dot{\varepsilon} \le 10 s^{-1}$) may be obtained from tests performed in tension using a servo-hydraulic machine. To obtain the required data at higher strain rates, it may be possible apply the double shear test (*if the behaviour of the material is isotropic*) as reported in Klepaczko (1994) and Rusinek and Klepaczko (2001) or compression test using Hopkinson bar.

By application of the method outlined above, the following constants have been found for *DH-36* and *Weldox 460-E* steels, Tables 3 and 4.

Conventional physical constants can be obtained from material handbooks, Table 5.

The strain rate and temperature effects on the modulus of plasticity B and the strain hardening exponent n for *DH-36* steel are shown in Fig. 4a and b. A decrease of the strain hardening exponent n is observed with both variables. At high strain rates the rate of strain hardening decreases due to thermal softening of material since the thermal effects are also included. Concerning variations of the total stress due to plasticity, as expected the total stress, $\bar{\sigma}$, increases with the strain rate and decreases with temperature.

In the case of *Weldox 460-E*, and comparing values with *DH-36*, it is observed that the strain hardening exponent n is more stable showing just a small decrease at high strain rate and high temperature, Fig. 5a and b. Therefore, this material seems to be more stable in comparison to *DH-36*, concerning at least plastic instabilities at high strain rates due to high local temperature increase.

Finally, the prediction of *RK* model in the form of the total equivalent stress vs. equivalent strain is shown for *DH-36* and *Weldox 460-E* steels in Fig. 6. Calculations were performed at room temperature for a wide range of strain rates and plastic deformation up to $\bar{\varepsilon}_p = 1.0$. In conclusion, the transition between isothermal and adiabatic conditions is well defined. The thermal softening of the material at high strain rates is well observed in Fig. 6 by comparison of isothermal and adiabatic strain hardening curves. Moreover, comparing the analytical predictions for both materials, it is observed that *Weldox 460-E* is less sensitive to the rate of deformation. The correct definition of the material softening is revealed as a key factor to simulate impact events propitious to induce plastic instabilities and failures (Borvik et al., 2002a; Arias et al., 2008; Rusinek et al., 2005, 2007b, 2008c).

Table 3
Constants determined for *DH-36* steel for *RK* model.

B_0 (MPa)	ν (−)	n_0 (−)	D_2 (−)	ε_0 (−)	σ_0^* (MPa)	m^* (−)	D_1 (−)
906.87 Eq. (4)	0.02	0.2 Eq. (5)	0.085	1.8×10^{-2} Eq. (7)	491.11 Eq. (8)	2.127	0.49 Eq. (6)

Table 4
Constants determined for *Weldox-460-E* steel for *RK* model.

B_0 (MPa)	ν (−)	n_0 (−)	D_2 (−)	ε_0 (−)	σ_0^* (MPa)	m^* (−)	D_1 (−)
983.59 Eq. (4)	0.107	0.175 Eq. (5)	0.052	1.8×10^{-2} Eq. (7)	100 Eq. (8)	1.031	0.49 Eq. (6)

Table 5
Physical constants for ferritic steels.

E_0 (MPa)	θ^* (−)	C_p (J kg K^{-1})	β (−)	ρ (kgm^{-3})
212	0.59	470	0.9	7800

3.2. The Johnson–Cook (JC) model

In order to compare the *RK* model, the Johnson–Cook (*JC*) constitutive relation (Johnson and Cook, 1983) is considered in this paper. This relation is commonly used in numerical analyses of dynamic processes (Mae et al., 2007; Smerd et al., 2005; Borvik et al., 2002b, 1999; Gupta et al., 2006, 2007; Arias et al., 2008; Rusinek et al., 2008b; Teng et al., in press). Considerable efforts have been made in the past to identify the material constants necessary to apply the model for variety of different metallic materials. This fact has enhanced the notorious diffusion of the model during the last two decades. In addition, it presents a simple formulation which can be easily manipulated analytically. The main drawback is multiplication of three terms depending respectively on strain, strain rate and temperature.

However, some progress in constitutive modeling applied in computer codes is evident. Since *JC* model is based on a phenomenological approach, it does not consider the flow stress as decomposed into two parts, the effective

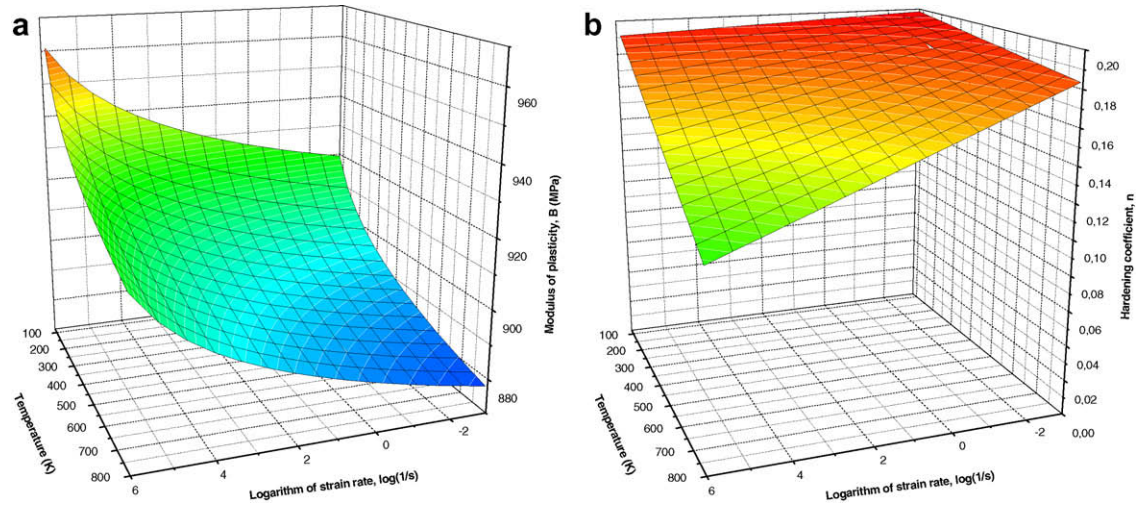

Fig. 4. Temperature and strain rate effects on plasticity of *DH-36* steel: (a) modulus of plasticity $B(\dot{\bar{\varepsilon}}, T)$; (b) strain hardening exponent $n(\dot{\bar{\varepsilon}}, T)$.

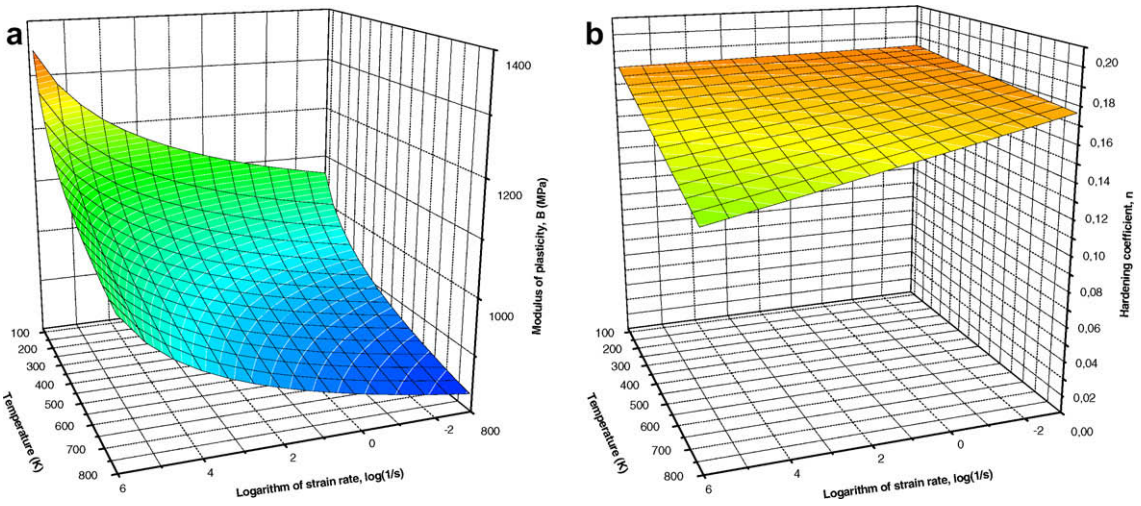

Fig. 5. Temperature and strain rate effect on *Weldox-460-E* steel: (a) modulus of plasticity; (b) strain hardening exponent.

stress and the "athermal" stress. This is the main difference with *RK* model and the previous considerations of Seeger (1957) and Klepaczko (1975). Moreover, strain hardening is defined as a power law, so called Swift hardening, but without taking into account the effect of strain rate and temperature. The constancy of the strain hardening exponent n in *JC* formulation is contrary to the experimental observations frequently made and reported for metals in many publications (for example, Rusinek et al., 2007a), Fig. 7. This fact rises considerable relevance especially in dynamic events susceptible to plastic instabilities, (Rusinek et al., 2005, 2007b, 2008c; Klepaczko 2005; Teng et al., 2007), frequently observed in impact events, (Rusinek et al., 2008c; Teng et al. 2007; Borvik et al., 2003). Moreover, it should be noticed that the constant logarithmic strain rate sensitivity $\beta = (\partial\bar{\sigma}/\log\dot{\bar{\varepsilon}}_{\mathrm{p}})_{\bar{\varepsilon}_{\mathrm{p}},T}$ introduced in the original version of the *JC* model is ineffective to define the strain rate sensitivity of most metals from quasi-static to high strain rates as reported by Rusinek et al. 2008c). See for example, Fig. 7. This assumption can be extended to other phenomenological constitutive relations, for example the Power Law formulation, (Rusinek et al., 2008c; Klepaczko, 1965), or Cowper and Symonds (1952), constitutive relation.

The explicit formulation of *JC* model defines the equivalent Huber–Misses stress, $\bar{\sigma}$, as three uncoupled terms where the first one defines the hardening dependency, the second one the strain rate sensitivity and the third one the temperature effects, Eq. (9).:

$$\bar{\sigma}(\bar{\varepsilon}^{\mathrm{p}}, \dot{\bar{\varepsilon}}^{\mathrm{p}}, T) = \left[A + B(\bar{\varepsilon}^{\mathrm{p}})^{n}\right]\left[1 + C\ln\left(\frac{\dot{\bar{\varepsilon}}^{\mathrm{p}}}{\dot{\varepsilon}_0}\right)\right](1 - \Theta^{\mathrm{m}}) \qquad (9)$$

where A is the quasi-static yield stress at $\dot{\bar{\varepsilon}}^{\mathrm{p}} = \dot{\varepsilon}_0$ and T = const., B is the modulus of strain hardening, n is the strain hardening exponent (material constant), $C = \beta$ is

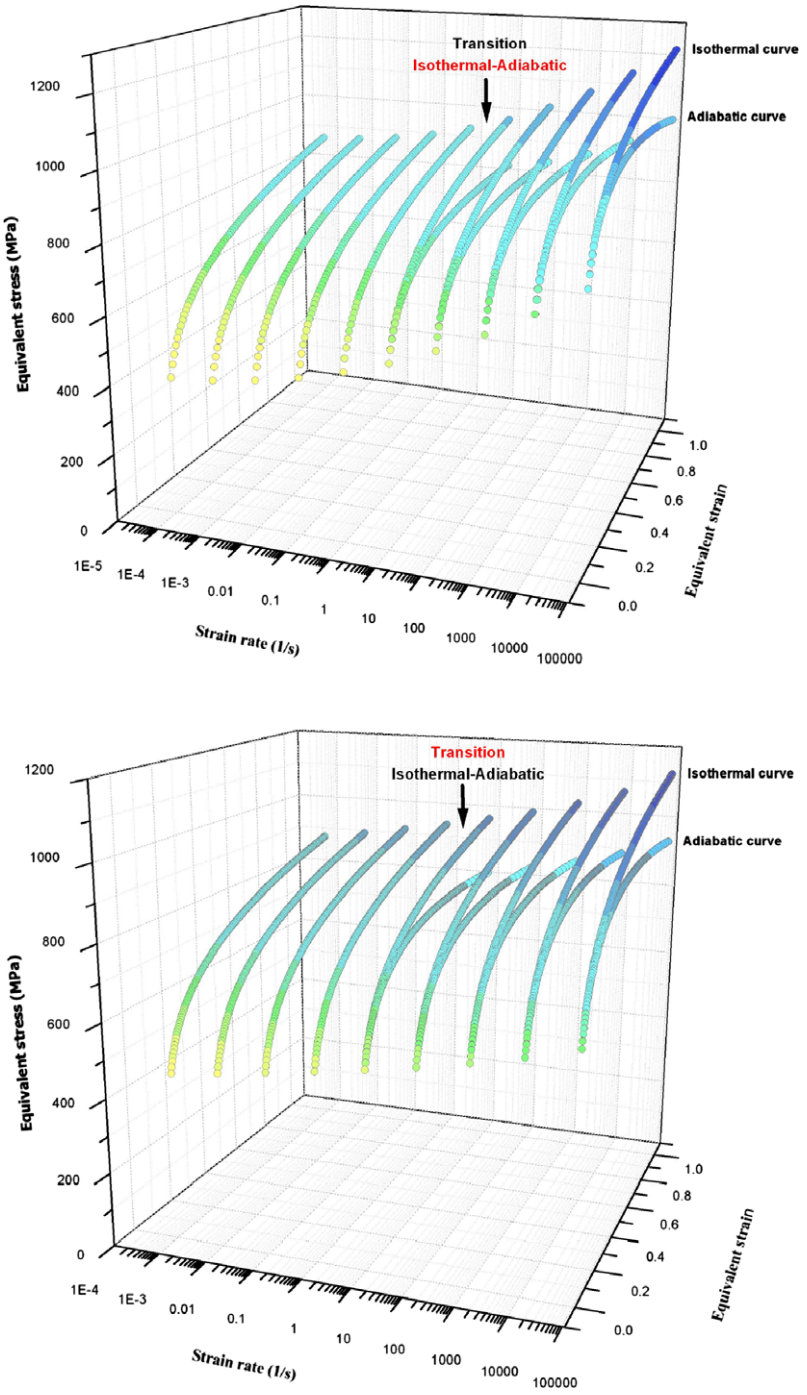

Fig. 6. Behaviour of *DH-36* steel (top) and *Weldox-460-E* steel (bottom) at different strain rates, adiabatic and isothermal conditions.

the strain-rate sensitivity, and m defines the temperature sensitivity; $\dot{\varepsilon}_0$ is the reference strain rate and Θ is the modified temperature given by:

$$\Theta = \frac{T - T_0}{T_m - T_0} \tag{10}$$

where T is the current temperature, T_0 is the initial temperature, and T_m is the melting temperature. As reported in Nemat-Nasser and Guo (2003) T_0 must be chosen as the lowest temperature of interest or the lowest temperature of experimental data available.

The following constants were used to approximate the thermo-visco-plastic behaviour of *DH-36* (Nemat-Nasser and Guo, 2003) and *Weldox 460-E* (Borvik et al., 1999; Arias et al., 2008) steels via *JC* model, Tables 6 and 7.

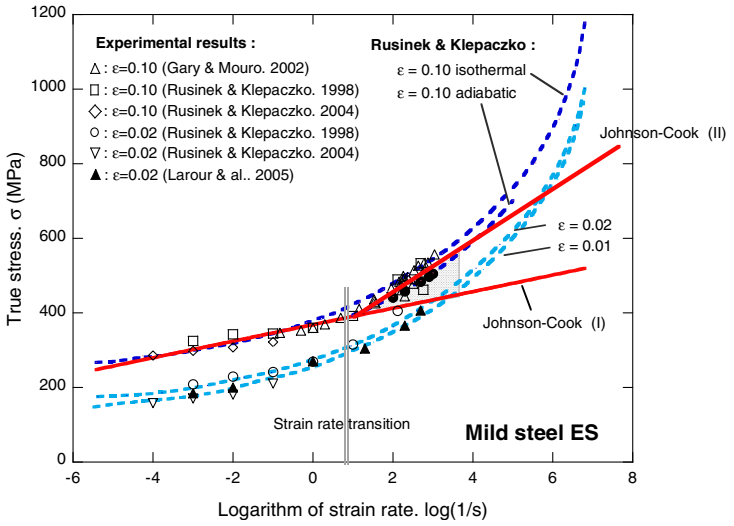

Fig. 7. Strain rate sensitivity definition in *RK* and other models for mild steel ES, comparison with experimental results.

More recently the *JC* constitutive relation, Eq. (9) has been modified by introduction of nonlinear terms in approximation of the rate sensitivity, (Johnson et al., 2006).This modified form is given below, Eq. (11):

$$\bar{\sigma}(\bar{\varepsilon}^{\mathrm{p}},\dot{\bar{\varepsilon}}^{\mathrm{p}},T)=\left[A+B(\bar{\varepsilon}^{\mathrm{p}})^{n}\right]\left[1+C_1\ln(\dot{\bar{\varepsilon}}^{\mathrm{p}})+C_2\ln(\dot{\bar{\varepsilon}}^{\mathrm{p}})^{C_3}\right]\left[1-T^{\mathrm{m}}\right] \tag{11}$$

where C_2 and C_3 are the new material constants. Because the strain hardening term is multiplied by the nonlinearly increasing second term, at high strain rates the parabolic stress–strain curves increase excessively at larger strains. This is in contradiction to experimental data for BCC metals and alloys.

Another model with some physical background, called *PB*, is analyzed. This model was introduced in Nemat-Nasser and Guo (2003, 1999); Nemat-Nasser and Isaacs (1997); Nemat-Nasser et al. (1999, 2001) and it is discussed in the following section.

3.3. The Physical Base (PB) model

This constitutive relation, as *RK* model, is based on the process of thermal activation with an additive decomposition of the total stress in agreement with Fig. 2. Thus, the total equivalent stress $\bar{\sigma}$ is defined by Eq. (12), in agreement with the considerations reported by Seeger (1957); Klepaczko (1975)

$$\bar{\sigma}=\sigma_{\mathrm{a}}+\sigma^{*} \tag{12}$$

The first component σ_{a} defines the athermal part independent on strain rate and temperature. The second stress component is the thermally activated part depending on strain rate and temperature. In comparison with *RK* model σ_{a} has the same standard name as introduced by Conrad (1964). In *PB* model, as mentioned previously, the internal stress depends only on the equivalent strain. Moreover, to take into account the strain hardening in *PB* formulation, a power law approximation is introduced, Eq. (13).

$$\sigma_{\mathrm{a}}=\mathrm{a}_1(\bar{\varepsilon}_{\mathrm{p}})^{n_1} \tag{13}$$

where a_1 is the material constant fitting the stress level and n_1 is the strain hardening exponent (assumed constant in this formulation). For *DH-36* steel the following values have been reported: $a_1 = 750$ MPa, and $n_1 = 0.25$, (Nemat-Nasser and Guo, 2003).

Several considerations may be important concerning this approach, Eq. (13), to describe the strain hardening evolution. The fact of assuming a strain hardening term independent on strain rate and temperature is in disagreement with experimental observations frequently published in the international literature (for example, Rusinek et al., 2007a), and many more publications. It is observed that strain hardening exponent depends on the strain rate and it is in addition coupled with temperature. This dependency is the key point when the constitutive relation is applied to analyze instabilities and failures. Using instability criterion in tension, Considère (1885), $(\partial\sigma_{\mathrm{a}}/\partial\bar{\varepsilon}_{\mathrm{p}})=\sigma_{\mathrm{a}}$ applied to a power strain hardening, as for *PB* case, the following relation is obtained, Eq. (14).

$$\bar{\varepsilon}_{\mathrm{p}}^{\mathrm{inst}}=n_1,\quad \sigma^{*}=0 \tag{14}$$

Using experimental observations reported in Dhulst and Even (2003), it is found that the instability strain or strain level at the maximum of true stress is not constant

Table 6
Constants defined for steel *DH-36* for *JC* model (Nemat-Nasser and Guo, 2003).

A (MPa)	B(MPa)	n (−)	$\dot{\varepsilon}_0$ (s^{-1})	C (−)	m (−)	T_0 (K)	T_{m} (K)
1020	1530	0.4	1×10^{-1}	0.015	0.32	50	1773

Table 7
Constants defined for steel *Weldox-460-E* for *JC* model (Borvik et al., 1999; Arias et al., 2008).

A (MPa)	B (MPa)	n (−)	$\dot{\varepsilon}_0$ (s^{-1})	C (−)	m (−)	T_0 (K)	T_{m} (K)
490	807	0.73	5×10^{-4}	0.012	0.94	296	1800

for all strain rates and temperatures but decreases when the strain rate increases. This phenomenon is faster at low temperatures due to more rapid thermal softening by adiabatic heating as it can be observed in the case of mild steel ES (mild steel), Fig. 8.

Therefore the value of n is not constant Fig. 9a–b for different temperatures. This behaviour can be considered true for temperatures not lower than 213 K, (Rusinek et al., 2007a), Fig. 9a.

It is observed in addition that the yield stress depends on the initial temperature. Thus the first material constant a_1 must depend on temperature, and because the yield stress is a function on strain rate (strain rate sensitivity), a_1 must depend also on the strain rate, Fig. 9a and b and Fig. 10.

Moreover, to approximate the stress dependency in terms of strain rate and temperature sensitivities, a second stress component is directly taken into *PB* formulation as introduced by Ono, (Ono, 1968), Eq. (14). This formulation is based on physical modeling by application of Arrhenius relation combined with Gibb's free energy formulation. Therefore the effective stress σ^* is defined in *PB* according to Ono (1968) and Kocks et al. (1975)

$$\sigma^* = \hat{\sigma}\left[1 - \left(-\frac{kT}{G_0}\ln\frac{\dot{\bar{\varepsilon}}_p}{\dot{\varepsilon}_r}\right)^{1/q}\right]1/p \tag{15}$$

The constants p and q define the profile of the short-range energy barrier to dislocation motion. Ono (1968)) and Kocks et al. (1975) suggested that $p = 2/3$ and $q = 2$ are suitable values for these constants for many metals. The parameter k/G_0 characterizes the temperature sensitivity of the material. Higher temperature sensitivity is associated with the higher value of k/G_0 whereas an increase of $(\dot{\varepsilon}_r)^{-1/q}$ corresponds to smaller strain-rate sensitivity. The threshold stress $\hat{\sigma}$ is the thermally activated obstacle strength at $T = 0$ K.

The constants for *DH-36* steel related to the effective stress are given in Table 8 (Nemat-Nasser and Guo, 2003).

Having identified the material constants for all models on the basis of experimental results (*RK, JC* and *PB* in the case of *DH-36; RK* and *JC* in the case of *Weldox 460-E*), a comparison is reported in the following sections of this document concerning the strain hardening and also the strain rate and temperature sensitivities.

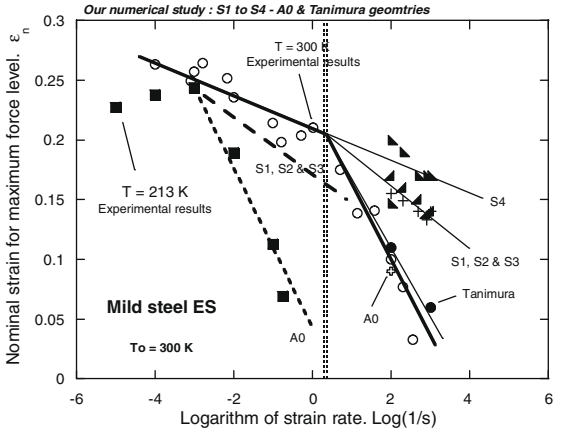

Fig. 8. Evolution of failure strain vs. strain rate at different initial temperatures (Rusinek et al., 2007a).

4. Validation of RK constitutive relation for modelling the thermo-viscoplastic behaviour of DH-36 and Weldox 460-E steels

In this section, the validation of the analytical predictions obtained using *RK* model is reported. The analysis is carried out in terms of strain rate and temperature sensitivities. For strain rate higher than $\dot{\bar{\varepsilon}}_p \geq 10\ s^{-1}$, the process is considered as adiabatic and the temperature increase is calculated for each increment of plastic deformation. Thus, the process of thermal softening can be estimated by analytical modeling.

4.1. Comparison of DH-36 behaviour between RK model and experimental results for a wide range of strain rates and temperatures

4.1.1. Strain rate sensitivity

The first comparisons are performed via analysis of strain rate effect, Fig. 11, in the range: $0.001s^{-1} \leq \dot{\bar{\varepsilon}}_p \leq 3000s^{-1}$. It is observed a good agreement between

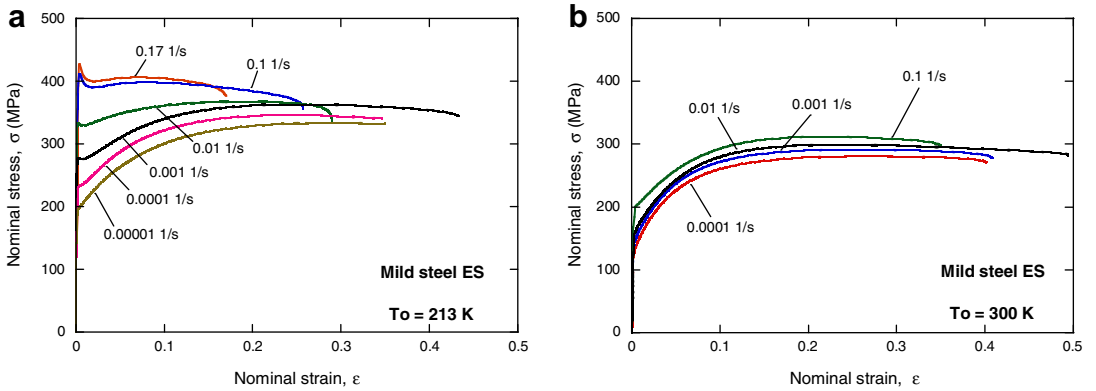

Fig. 9. Strain rate and temperature effects on strain hardening; (a) low temperature; (b) room temperature, experimental results (Rusinek et al., 2007a).

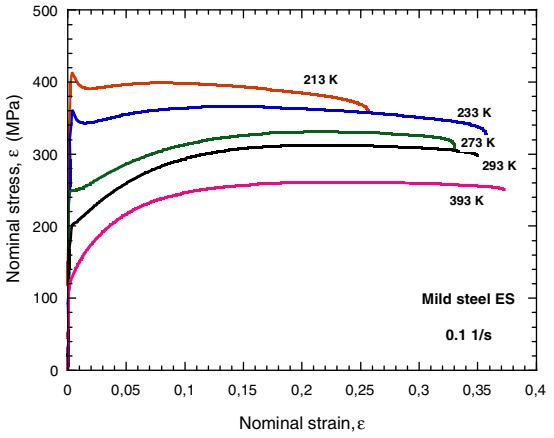

Fig. 10. Temperature effect on flow stress for a mild steel at 0.1 1/s; experimental results (Rusinek et al., 2007a).

Table 8
Physical constants for*DH-36* steel, Eq. (14) (Nemat-Nasser and Guo, 2003).

$\hat{\sigma}$ (MPa)	kT/G_0 (−)	$\dot{\varepsilon}_r$ (1/s)	q (−)	p (−)
1500	6.6E-5	2E10	2	2/3

experimental results and *RK* predictions for the entire range of strain rates, including the thermal softening of the material for high strain rate, higher than $\sim 10\,s^{-1}$. In the case of $\dot{\bar{\varepsilon}} = 3000s^{-1}$ some differences between analytical predictions and experiments take place at the beginning of loading due to inertia effect.

A comparison has also been performed for a jump of strain rate from quasi-static to intermediate or high strain rates, Fig. 12. It is observed a good agreement with experimental results. Some differences appear just after the jump of strain rate due to inertia effect.

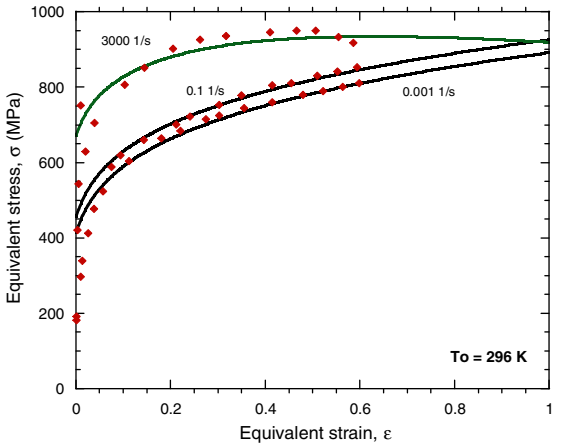

Fig. 11. Strain rate effect on plastic flow for *DH-36* steel. Analytical prediction by *RK* model and comparison with experimental results (Nemat-Nasser and Guo, 2003).

It is observed for the analytical predictions of *RK* model that the stress level is higher during a jump of strain rate from quasi-static loading to higher strain rate than during continuous loading at the higher strain rate. This happens because the process is considered first as isothermal, which is not the case for continuous plastic deformation at strain rate level of $3 \times 10^3\,s^{-1}$. After change of strain rate the process is adiabatic and the temperature is continuously increasing during plastic deformation. Then, a thermal softening of the material is observed inducing a stress level decrease.

4.1.2. Temperature sensitivity

To validate *RK* model for a wide range of temperatures, experimental results published in Nemat-Nasser and Guo (2003) were analyzed. During the test the initial temperature was varied from 77 K $\leqslant T_0 \leqslant$ 800 K for quasi-static and high strain rate deformation. As it was discussed previously, the strain aging takes place depending on the strain rate level, Fig. 13. However, *RK* model can not reproduce such behaviour of materials and the predictions are limited to the adiabatic temperature increase without strain aging effect, Fig. 13.

Anyway, a good agreement between experiments and analytical predictions for all ranges of strain rates and temperatures is observed. The difference takes place only for the domain of strain aging temperatures. However, for high strain rate, $\sim 10^3\,s^{-1}$, the strain aging disappears for the range of temperatures considered and the analytical prediction is totally in agreement with experiments, Fig. 13d. A small difference concerning the flow stress between experiments and *RK* model is also observed at low strain rates and low temperatures. However, this difference decreases when the strain rate increases, Fig. 13c and d.

4.2. Comparison of Weldox 460-E behaviour between RK model and experimental results for a wide range of strain rates and temperatures

4.2.1. Strain rate sensitivity

In the following curves, a comparison is reported between analytical predictions using *RK* model and experimental results at different strain rates (Børvik et al., 2001), Fig. 14a and b. A satisfactory agreement is observed with experimental results. It is also observed that thermal softening of the material is well defined in the case of strain rate higher than $\dot{\bar{\varepsilon}}_p \geq 10\,s^{-1}$.

In addition, a satisfactory agreement with experiments was also found concerning the strain rate sensitivity for different levels of plastic strain. It is found a linear relation of the flow stress with the logarithm of strain rate until a certain strain rate level is reached, $\dot{\bar{\varepsilon}}_p \approx 10^4\,s^{-1}$ Fig. 15. In the case of strain rate level larger than $\dot{\bar{\varepsilon}}_p \approx 10^4\,s^{-1}$, the relation between the flow stress and the logarithm of strain rate predicted by the *RK* model is highly non linear, Fig. 15.

4.2.2. Temperature sensitivity

Concerning the temperature sensitivity, Fig. 16, as previously reported for *DH-36* steel, *Weldox-460-E* steel shows

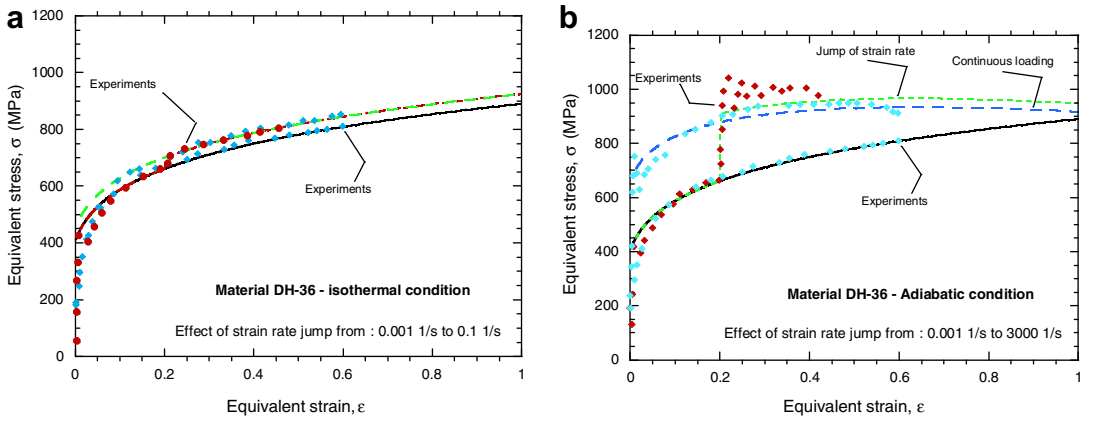

Fig. 12. Jump of strain rate effect on the macroscopic flow stress for *DH-36* steel. Analytical prediction by *RK* model and comparison with experimental results (Nemat-Nasser and Guo, 2003).

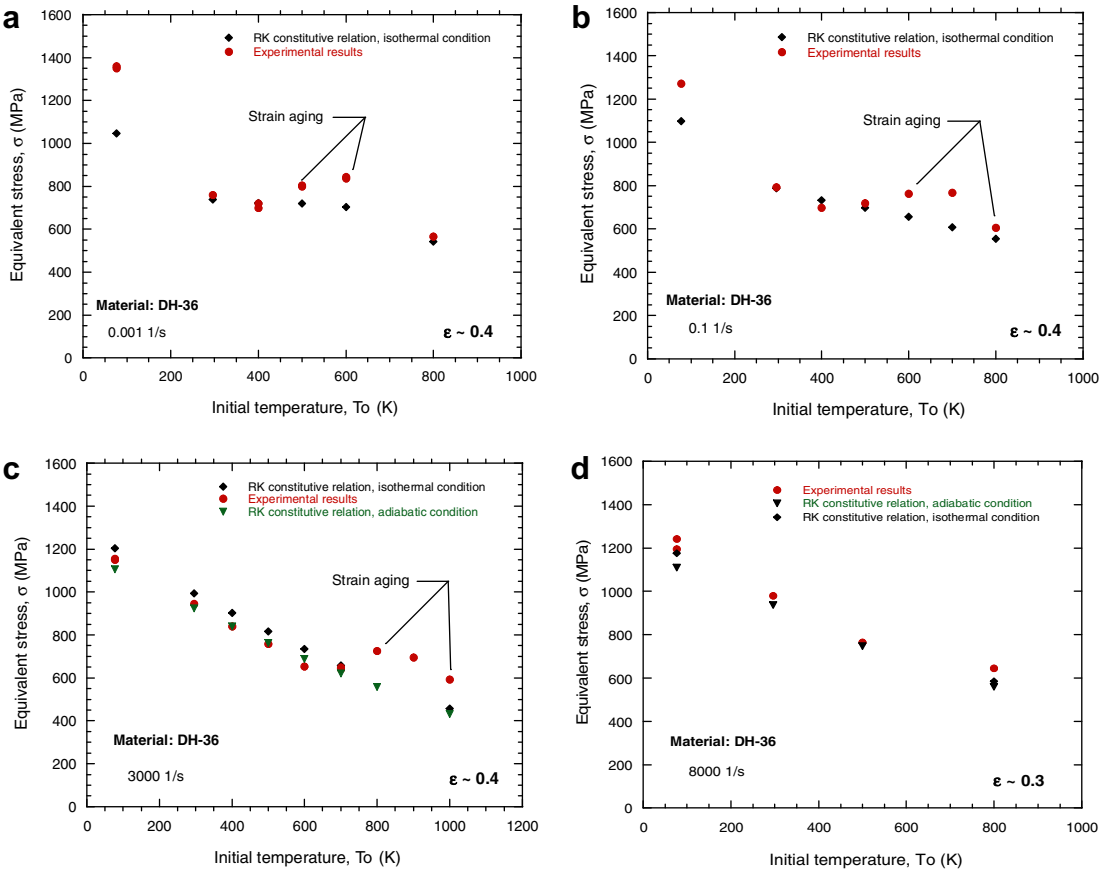

Fig. 13. Temperature effects predicted by *RK* model and comparison with experimental results at different strain rates (Nemat-Nasser and Guo, 2003); (a) 0.001 1/s; (b) 0.1 1/s; (c) 3000 1/s; (d) 8000 1/s.

the strain aging effect within the following temperature range, $400 < T_0 < 800$ K. Anyway, the agreement of the model predictions with experiments can be assumed as satisfactory.

5. Comparison between RK, PB and JC constitutive relations for modelling the thermo-viscoplastic behaviour of DH-36 steel

In the case of *DH-36*, *RK*, *PB* and *JC* constitutive relations are considered to define its thermo-viscoplastic behaviour. A first comparison is performed for *RK* and *PB* models concerning the internal stress and the effective stress as a function of increasing strain rate, Fig. 17.

It is observed that using the thermal activation decomposition, the effective stress σ^* is reduced for low strain rate if the temperature is larger than $0.4\,T_m$, Fig. 17. This temperature transition increases at high strain rates. However a difference is observed between these two models concerning the effective stress intensity, Figs. 17 and 18. For *RK* model and quasi-static loading the effective stress is close to zero. For *PB* model the effective stress, which defines the thermal activation, is equal to 161 MPa. Thus the thermally activated contribution to stress for *PB* model is assumed as dominant during quasi-static loading. Therefore, this stress component is higher than half of the internal stress which is mainly related to the microstructure evolution as discussed in Rusinek et al. (2007a).

The models can be analyzed via definition of the activation volume

$$V_a^* = \frac{1}{\sigma^*}\int V^*(\sigma^*)\mathrm{d}\sigma^* \tag{16}$$

where V_a^* is the activation area. It is observed that the effective stress increases with the decrease of the thermal activation volume, Fig. 19. It means that when the effective stress is large, as for *PB* model, the activation volume is small. Applying the experimental results for *DH-36* steel, Fig. 20d, it is possible to state that the activation volume, or rate of the strain rate sensitivity $\beta = (\partial\sigma^*/\partial \ln \dot{\varepsilon})_T$, appears for strain rate close to $\dot{\bar{\varepsilon}}^p \approx 10^2\ \mathrm{s}^{-1}$. This strain rate corresponds to the transition from isothermal to adiabatic conditions.

The next comparison is performed in terms of strain rate and temperature sensitivities for *RK*, *PB* and *JC* models,

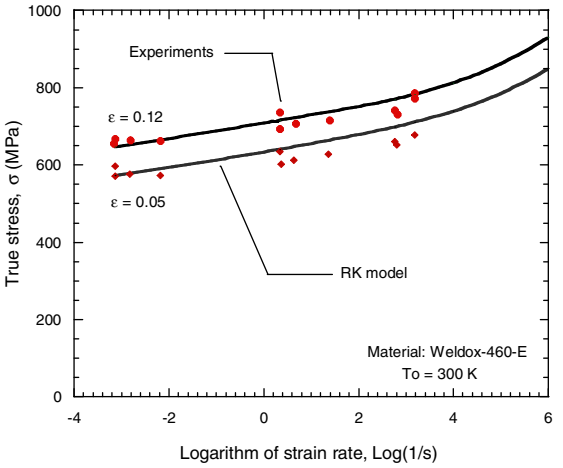

Fig. 15. Comparison between experimental results (Børvik et al., 2001) and approximation by *RK* model for two levels of strain vs. log of strain rate.

Fig. 20. It is found that *PB* and *RK* models give better results in comparison with *JC* model for low and intermediate strain rates. However, in dynamic loading the predictions are very close for all of them, Fig. 20c. A comparison is also obtained concerning the strain rate sensitivity for all strain rates applied during experiments for an imposed strain level, Fig. 20d. In this case, a better agreement is also found with *RK* and *PB* in comparison with *JC* model. This occurs in the case of *JC* due to the linear strain rate sensitivity β definition in Eq. (9).

Comparisons between the three models, *JC*, *PB* and *RK*, are also performed for all temperatures applied during experiments, Fig. 21. Concerning this problem, all models allow to predict the temperature dependency of flow stress. However, at high strain rates and low temperatures, *RK* model defines better the material behaviour, Fig. 21c. In this domain *PB* and *JC* models introduce an overestimation of the stress level. On the contrary, at low strain rates and

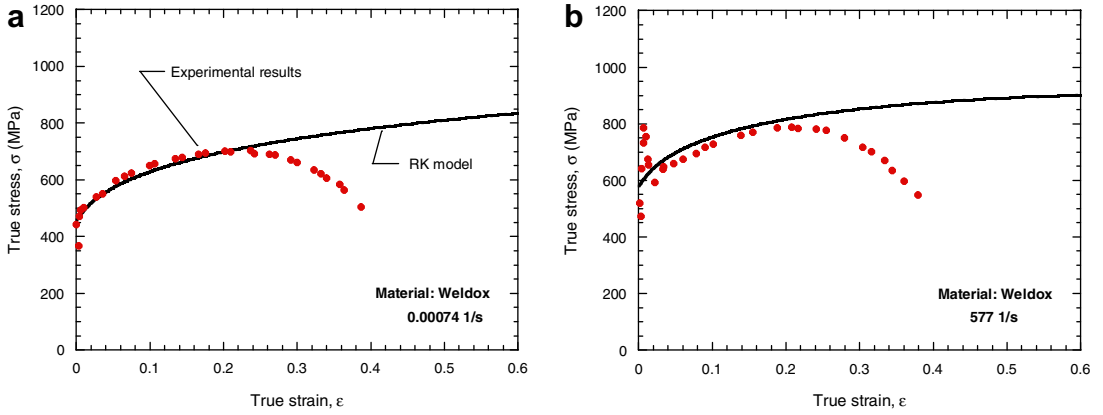

Fig. 14. Comparison between experimental results and *RK* model for *Weldox-460-E* at room temperature, experimental results by Børvik et al. (2001); (a) $0.0074\ \mathrm{s}^{-1}$; (b) $577\ \mathrm{s}^{-1}$.

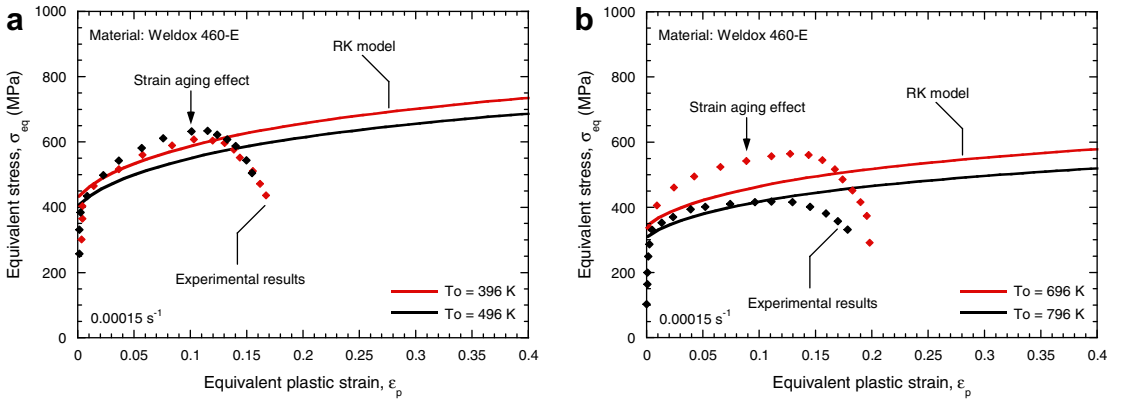

Fig. 16. Temperature sensitivity of flow stress for quasi-static tests for two strain levels using *RK* model, comparison with experiments (Børvik et al., 2001); (a) strain level 0.05; (b) 0.1.

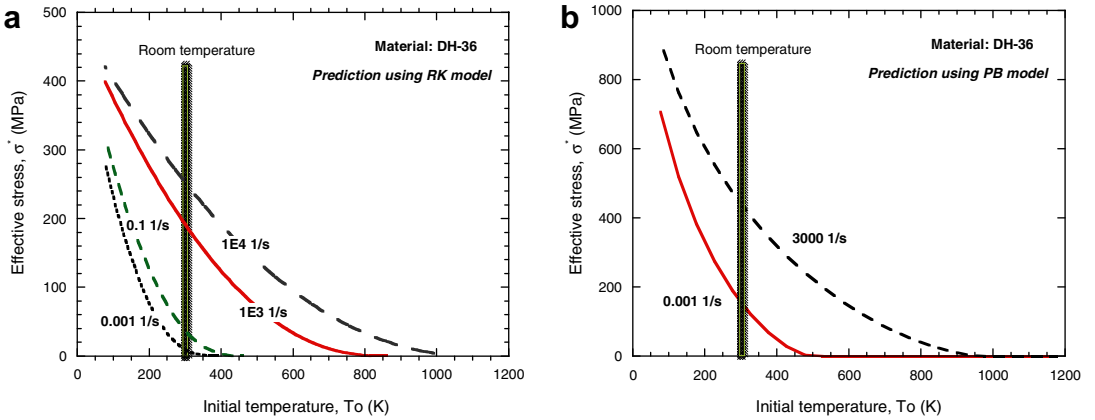

Fig. 17. Evolution of the effective stress due to thermal activation vs. temperature at different strain rates; (a) *RK* model; (b) *PB* model.

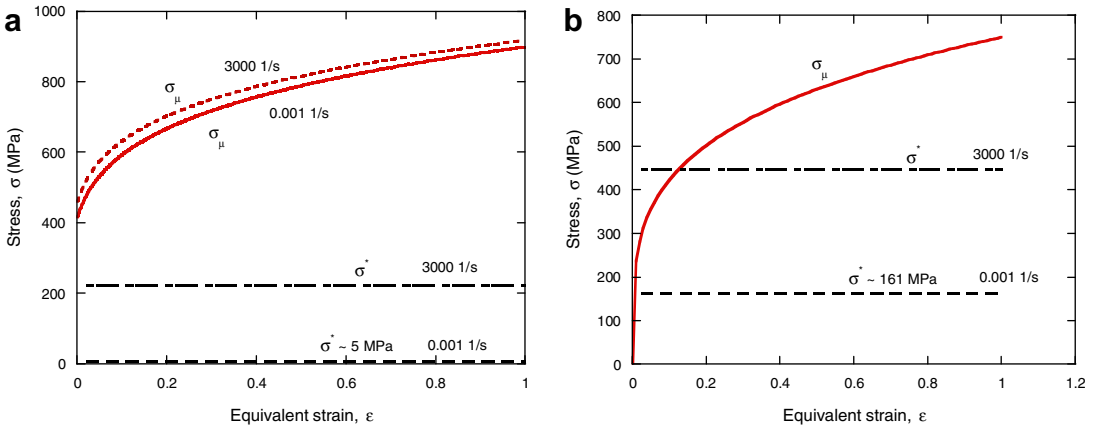

Fig. 18. Effect of the strain rate on the internal stress: (a) *RK* model, (b) *PB* model.

low temperatures *JC* and *PB* models define better the material behaviour, Fig. 21a. For intermediate strain rates, *PB* and *RK* models give better agreement with experiments in comparison with *JC* relation, Fig. 21b.

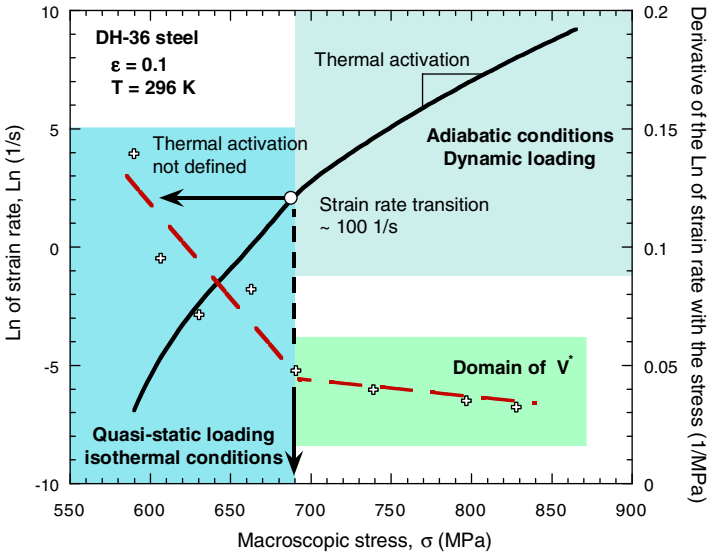

Fig. 19. Evolution of activation volume with total stress.

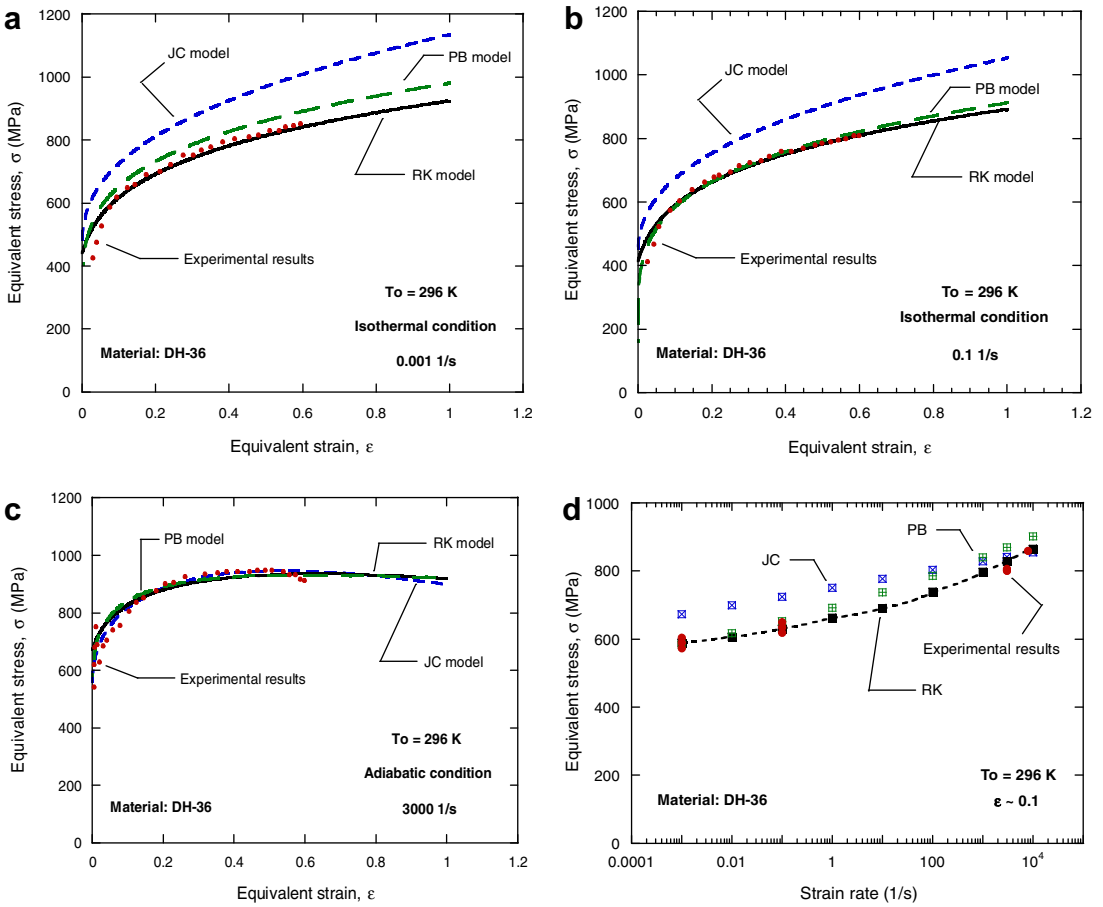

Fig. 20. Comparison of constitutive relations with experimental results for *DH-36* steel.

6. Comparison between RK and JC constitutive relations for modelling the thermo-viscoplastic behaviour of Weldox 460-E steel

Fig. 22a–d considers the evolution of strain hardening for different strain rate levels. The strain rate during experiments varied in the range of $0.0074s^{-1} \leq \dot{\bar{\varepsilon}}^{p} \leq 1512\ s^{-1}$. A satisfactory agreement of *RK* model with experiments is observed for all strain rates and temperatures considered, Fig. 22. *JC* model overestimates the flow stress at large deformation and it does not define correctly the thermal softening of the material in adiabatic conditions.

Subsequently it is analyzed the temperature sensitivity comparing the analytical predictions of the models with experimental results (Børvik et al., 2001). The comparison was performed for strain rate $\dot{\bar{\varepsilon}}_{p} = 5 \cdot 10^{-4}\ s^{-1}$ and temperature varying in the limits: $300\ K \leqslant T_0 < 800\ K$, Fig. 23. It is observed that *RK* model shows better agreement with experiments than *JC* model, especially for $\varepsilon_p = 0.1$. Fig. 23b. However, differences between the analytical predictions and the experiments take place for both models due to strain aging effect showed by this material.

7. Numerical simulation of perforation by application of RK and JC models

Impact perforation of steel plates was widely studied in the last decades due to the applications necessary in several engineering fields like aeronautics, automotive or military industries (Borvik et al., 1999; 2002a,b; 2003; Gupta et al., 2006, 2007; Arias et al., 2008; Rusinek et al., 2008b, 2008c; Teng et al., in press; Piekutowski, 2001; Chocron et al., 2001; Forrestal and Piekutowski, 2000; Dey et al., 2004; Børvik et al., 2005; Chocron et al., 2006; Teng and Wierzbicki, 2006; Voyiadjis and Abu Al-Rub, 2006; Rodríguez-Martínez et al., 2008). Several works can be found in the international literature dealing with different aspects of the perforation processes, for example, projectile geometry (Borvik et al., 2002a,b; Gupta et al., 2006, 2007; Arias et al., 2008; Rusinek et al., 2008b), target thickness, (Borvik et al., 2003), constitutive relation (Rusinek et al., 2008c), failure criterion (Teng and Wierzbicki, 2006), or material optimization, (Dey et al., 2004).

The necessity of the analysis of this kind of impact events is derived from the application of *DH-36* and *Weldox 460-E* steels as structural protection in, for example, fast boats or submarines. Such constructions may be subjected

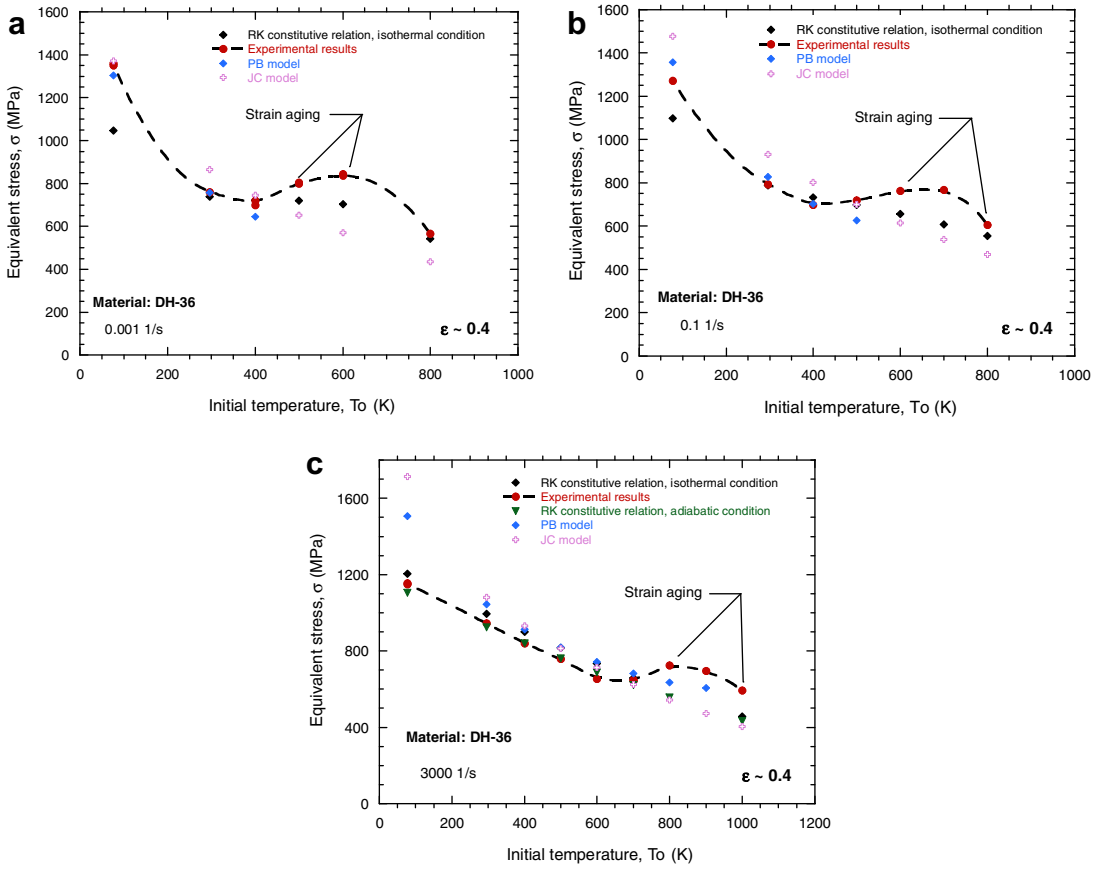

Fig. 21. Comparison between experiments (Nemat-Nasser and Guo, 2003) and models used in this study, *JC*, *PB* and *RK*.

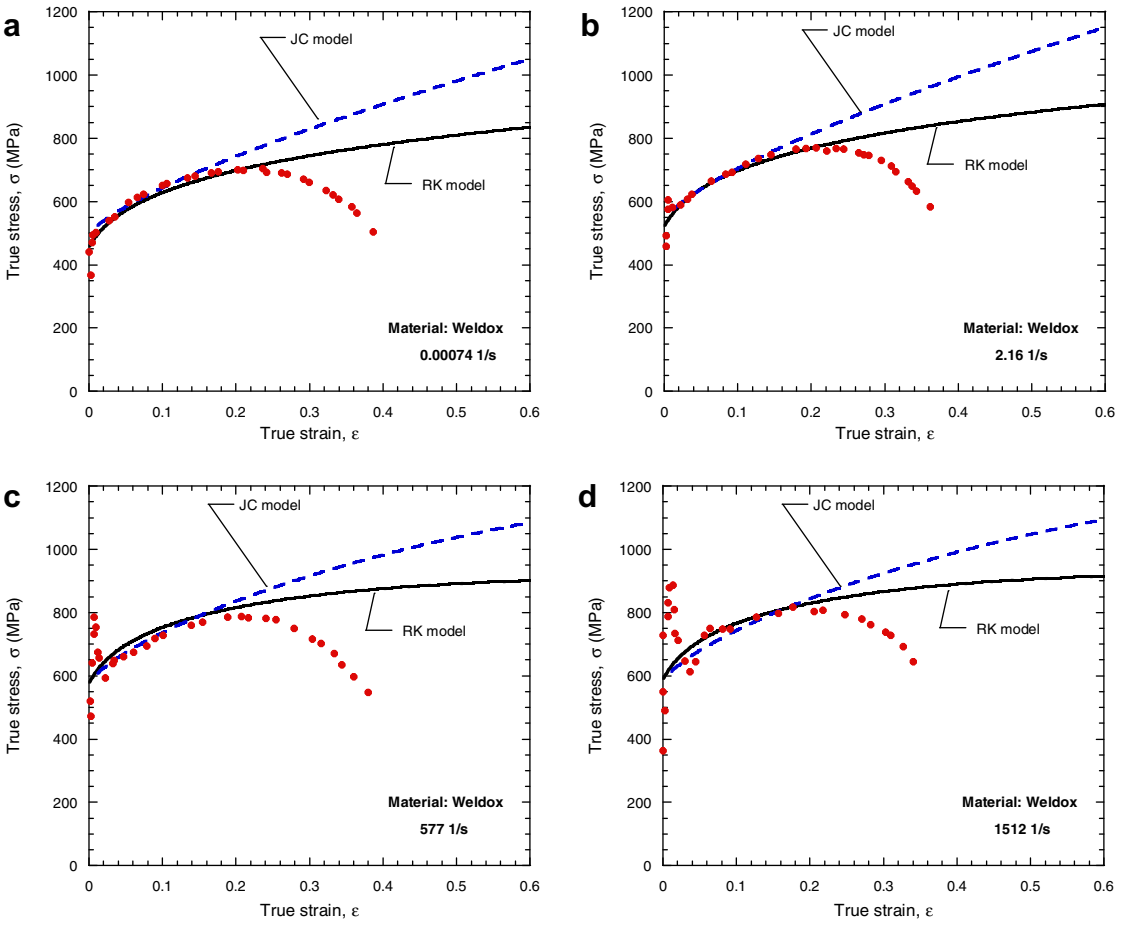

Fig. 22. Comparison between experimental results and *RK* model for *Weldox-460-E*, experimental results published in Børvik et al. (2001); (a) 0.0074 s^{-1}; (b) 2.16 s^{-1}; (c) 577 s^{-1}; (d) 1512 s^{-1}.

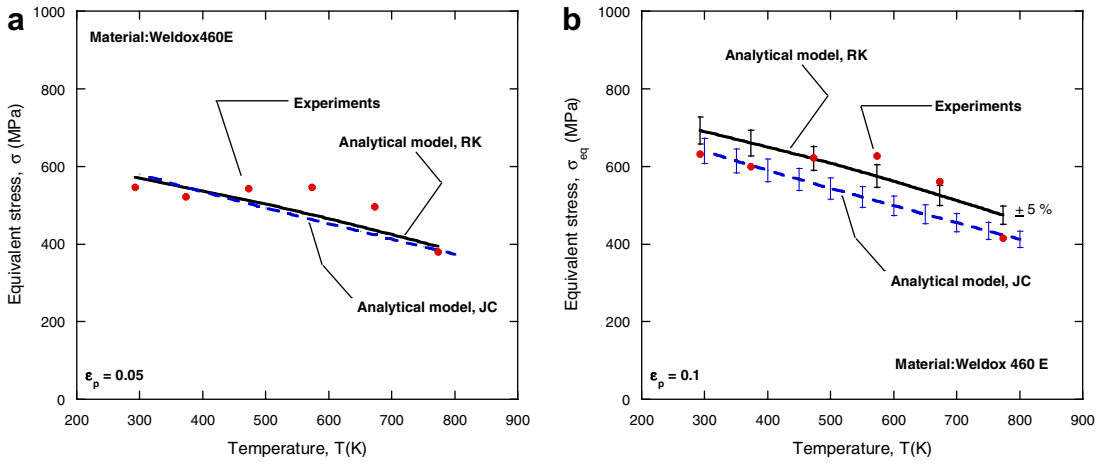

Fig. 23. Temperature sensitivity of flow stress in quasi-static condition for different strain levels, experiment (Børvik et al., 2001), *RK* and *JC* models; (a) strain level 0.05; (b) strain level 0.1.

to impulsive and explosive loads. Resistance to impact events is strongly related to strain hardening, strain rate and temperature sensitivities, as reported by Rusinek et al. (2008c). Therefore the use of an adequate constitutive relation to define the target behaviour is crucial. This section is devoted to numerical analyses focused on differ-

ences introduced by the constitutive relations, *RK* or *JC*, when applied to analyze the perforation of *DH-36* and *Weldox 460-E* plates. Special interest is focused on the effect of initial temperature. It is well known that marine vessels can be subjected to a wide range of environmental temperatures, which can oscillate from 313 K in equatorial seas to 213 K in both Earth Poles.

7.1. Numerical configuration

The numerical configuration used is based on the experimental set-up originally developed by Borvik et al. (2002a). In that case, *Weldox 460 E* steel plates were subjected to perpendicular impact by conical projectiles. The circular target plate had the following dimensions: diameter $\phi_t = 500$ mm and thickness, $t = 12$ mm. The conical projectiles had the mass of $M_p = 0.2$ kg and the nose angle, $\theta \approx 18.5°$, Fig. 24. The projectiles were oil quenched to reduce its erosion during impact.

In order to simulate impact events, an axi-symmetric configuration is traditionally used. This simplification of the problem has provided good results in terms of ballistic limit, failure time and energy absorbed by the plate for several projectile-plate configurations, (Borvik et al., 1999, 2002a,b; 2003; Gupta et al., 2006, 2007; Arias et al., 2008; Rusinek et al., 2008b; Børvik et al., 2005; Teng and Wierzbicki, 2006; Voyiadjis and Abu Al-Rub, 2006). However, recently Rusinek et al. (2008c) have noticed the convenience of using 3D approach to simulate particular aspects of the problem, mainly related to petalling, since this failure mode a is non-symmetric process. In the numerical simulations reported in the present work also 3D numerical approach was used. The target was meshed with 8 nodes hexahedral elements (C3D8R) and 4 nodes tetrahedral elements, (C3D4). The zone directly affected by impact was meshed using 36 hexahedral elements along thickness. The tetrahedral elements were used to define successive transition zones as one moves away from the center of the plate. This procedure was assumed in order to reduce the number of elements along thickens. Therefore the final calculus time is reduced without loss of accuracy. The projectile was assumed as a rigid body

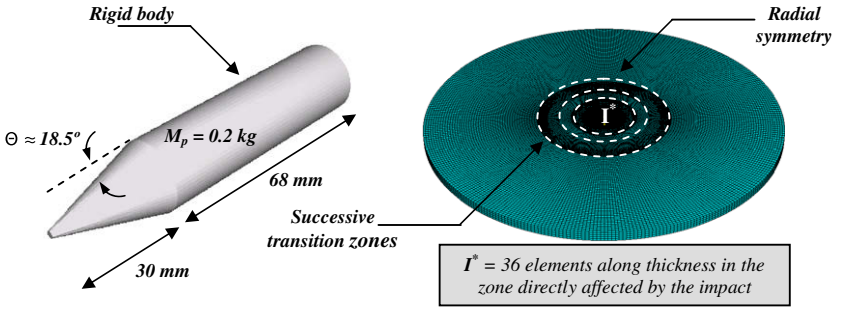

Fig. 24. Model configuration for numerical simulations; (a) Projectile dimensions (b) Target mesh.

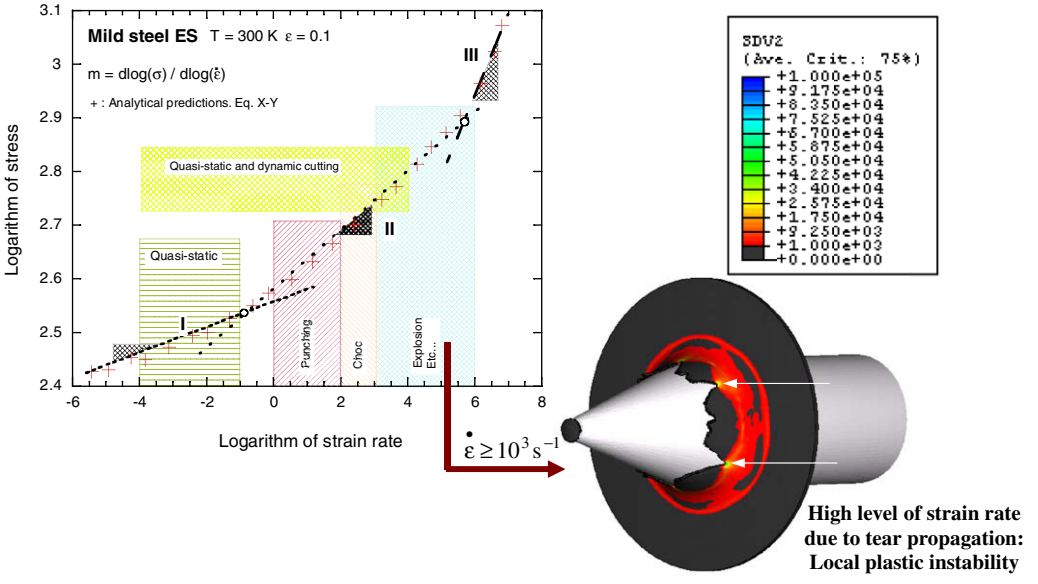

Fig. 25. Strain rate sensitivity for high velocity impact perforation, ES steel (mild steel). Strain rate contours during perforation for sheet of mild steel (Rodríguez-Martínez et al., 2008).

in agreement with the experimental observations previously commented (Borvik et al., 2002a).

To analyze perforation it is necessary to assume a failure criterion. In this case the effective failure strain $\varepsilon_f^p = 1$ was assumed as such criterion. This value comes from combination of the *RK* constitutive relation with the generalized Considère's criterion, $(d\bar{\sigma}/d\bar{\varepsilon}_p) = \bar{\sigma}$, (Considère, 1885). This procedure was previously applied by Rusinek et al. (2008c) and Rodríguez-Martínez et al. (2008) using the same value of the failure strain for the mild steel ES. Using the same procedure, different values of failure strain were tried for the three initial temperatures considered, (T_{01} = 200 K, T_{02} = 296 K, T_{03} = 400 K), but the differences found were reduced and only one value $\varepsilon_f^p = 1$ was used during the simulations. The friction coefficient assumed during the numerical simulations was μ = 0.05, this value has been previously used for example in Borvik et al. (2002b); Arias et al. (2008); Rusinek et al. (2008b).

7.2. A role of constitutive relation

Both, *RK* and *JC* models have been applied to define the material behaviour during the simulations in order to analyze one constitutive relation with some physical background (*RK*) and another purely phenomenological (*JC*). Moreover *JC* constitutive relation has been widely used to define material behaviour when subjected to impact events and is commonly pre-implemented in most of the FE commercial codes, including ABAQUS/Explicit. However, the implementation of *RK* model has been carried out by the present authors using the fully-implicit algorithm originally proposed by Zaera and Fernández-Sáez (2006). This algorithm belongs to the class called return mapping, which are robust and widely used in practice (Simo and Ortiz, 1985; Simo and Taylor, 1986). The algorithm was previously implemented into *RK* scheme in order to simulate impact problems like dynamic tension test (Rusinek et al., 2005, 2008a), dynamic ring expansion (Rusinek at al., 2007b) and perforation processes (Rusinek et al., 2008c). In the previous numerical work, (Rusinek et al., 2008c), several constitutive relations were evaluated, namely: *PL*, *JC* and *RK*. They represent different approximations of strain rate sensitivities, which affect the perforation process of mild steel plates. In application of *PL* and *JC* constitutive relations it was necessary to identify different sets of material constants to reproduce the material behaviour in the whole range of strain rates considered, $10^{-3}s^{-1} \le \dot{\bar{\varepsilon}}_p \le 10^{6}s^{-1}$. However, for *RK* model just one set of constant was sufficient. This is the main reason why appreciable differences appear for the numerical results obtained by each constitutive relation for the same boundary-value problem. The closest results to experiments in terms of ballistic limit, failure time, force-time history and failure mode were found for simulations with

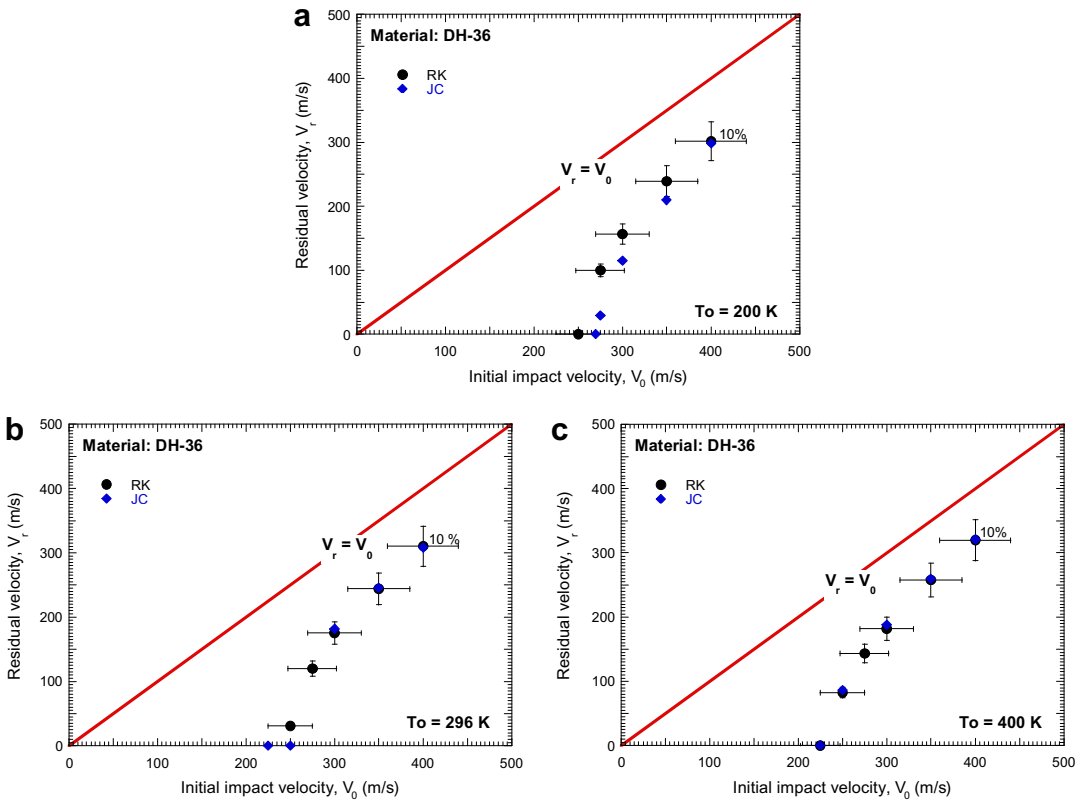

Fig. 26. Numerical simulation of residual velocity using *RK* and *JC* models at different initial temperatures; (a) T_o = 200 K, (b) T_o = 296 K, (c) T_o = 400 K.

RK model. It must be noticed that *RK* constitutive relation presents the advantage of predicting the material behaviour when subjected to high initial temperature and strain rate levels since it introduces variable strain hardening in general form $n = n_0 f(\dot{\bar{\varepsilon}}_p, T)$ as previously discussed in this paper, where f <∗> is the weight function. Moreover, the strain rate level locally reached by the material for the range of impact velocities is estimated in the limits of $10^3 s^{-1} \leq \dot{\bar{\varepsilon}}_p \leq 10^6 s^{-1}$, (Rusinek et al., 2008b, 2008c), Fig. 25. This strain rate level was also observed in Rodríguez-Martínez et al. (2008) via the numerical approach for sheets of mild steel ES perforated by conical projectiles, Fig. 25.

The next step after evaluating the effect of critical failure strain and strain rate sensitivity definition in impact events is to analyze the influence of constitutive relation when the target is subjected to different initial temperatures.

7.3. The case of DH-36 steel

The lowest temperature applied during the simulations was T_{01} = 200 K, which corresponds to the minimum temperature that marine structures can be subjected in extreme environmental conditions. The intermediate temperature was assumed as T_{02} = 296 K, which corresponds to standard temperature condition, and the highest T_{03} = 400 K, as the maximum temperature that marine structures are usually subjected.

The first consideration in the numerical analysis was to evaluate the ballistic limit and the residual velocity predicted by each constitutive relation for the three initial temperatures considered. It should be noticed that the curves residual velocity vs. initial velocity obtained from the numerical simulations Fig. 26, present the typical parabolic profile of dynamic perforation events, (Borvik et al., 2002a,b; Gupta et al., 2006, 2007; Arias et al., 2008; Rusinek et al., 2008b; Voyiadjis and Abu Al-Rub, 2006). It is also shown in Fig. 26 how the ballistic limit increases, close to $\Delta V_{bl} \approx 70$ m/s, from T_0 = 400 K to T_0 = 200 K. This is found for both constitutive relations considered, which notice the relevance of the initial temperature on the behaviour under impact and perforation of *DH-36* steel.

In the cases of T_0 = 400 K and T_0 = 296 K, the ballistic limit and the residual velocity predicted by both constitutive relations for the range of impact velocities considered do not differ by more than 10%, Fig. 26a and b. For both initial temperatures the JC model estimates a higher ballistic limit, Fig. 26. But these differences notably augment in the case of T_0 = 200 K for which the ballistic limit predicted by both constitutive relations presents a variation range of $\Delta V_{bl} \approx 500$ m/s showing the relevance of procuring a good definition of the *DH-36* behaviour especially in terms of temperature sensitivity.

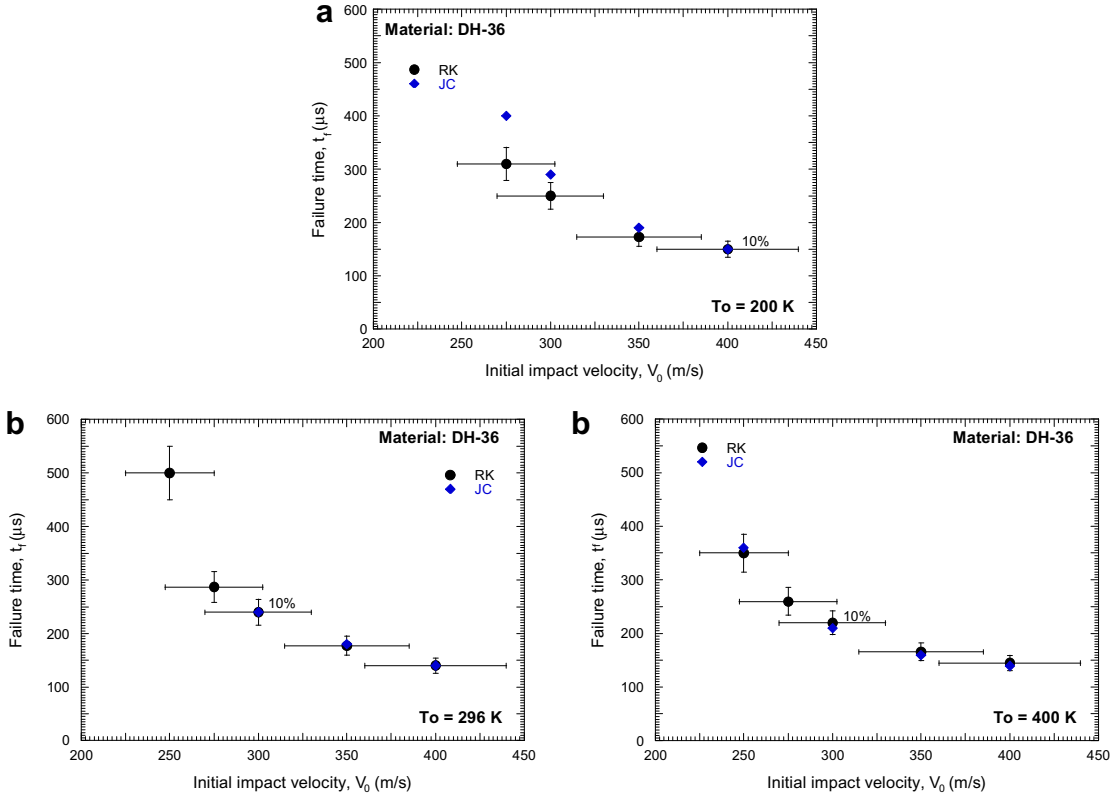

Fig. 27. Numerical simulation of failure time using *RK* and *JC* models at different initial temperatures; (a) V_o = 400 m/s and T_o = 200 K, (b) V_o = 300 m/s T_o = 296 K, (c) V_o = 250 m/s and T_o = 400 K.

Similar conclusions can be obtained analyzing the values of failure time obtained from the numerical simulations, Fig. 27. The evolution of failure time with the impact velocity for all the constitutive relations used presents the classical parabolic profile of perforation. This is in agreement with the experimental and numerical observations reported in Borvik et al. (2002a,b); Gupta et al., (2006, 2007); Arias et al. (2008); Rusinek et al. (2008b); Voyiadjis and Abu Al-Rub (2006). JC constitutive relation predicts the longest failure time, and the differences predicted are notably augmented in the case of $T_0 = 200$ K.

Contours of stress level are shown in Fig. 28 for $V_0 = 300$ m/s and $T_0 = 400$ K for both constitutive relations analyzed. Stress wave propagation is clearly visible due to the fully 3D numerical configuration used. The reduced petalling process appearing when large thickness plates are impacted by conical projectiles is well predicted in agreement with the experimental observations reported in Borvik et al. (2002a); Dey et al. (2004).

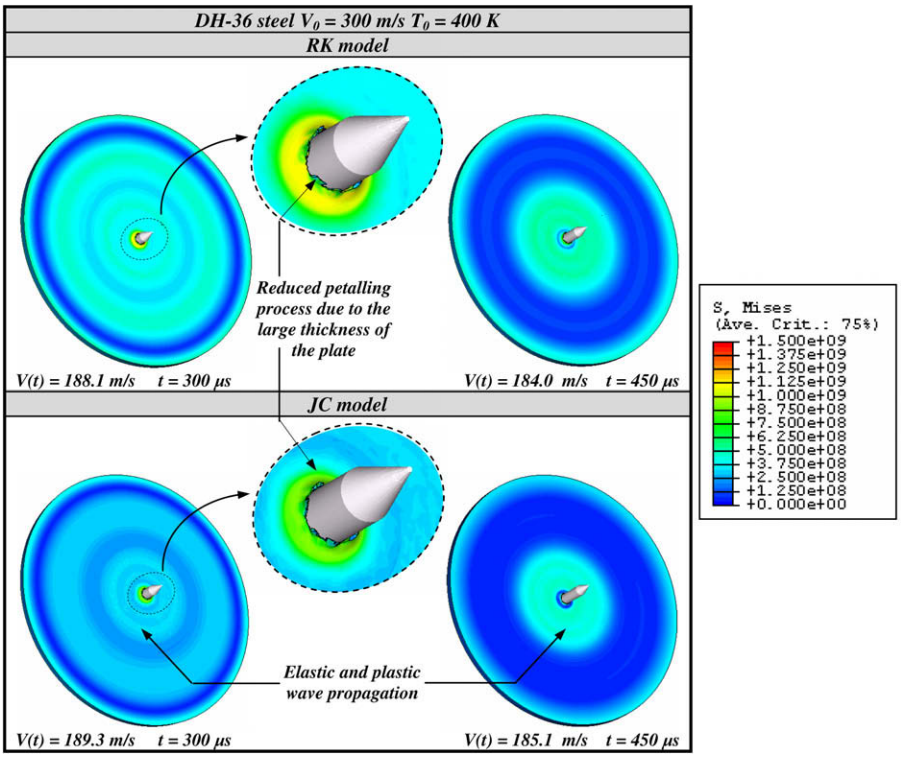

Fig. 28. Equivalent stress contours during the perforation process for *RK* and *JC* models. $V_0 = 300$ m/s, $T_o = 400$ K.

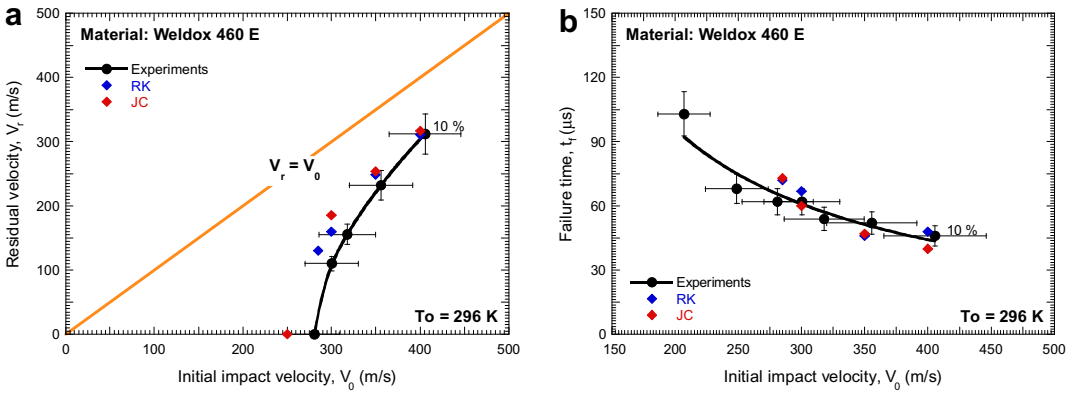

Fig. 29. Numerical estimation and comparison with experimental results (Borvik et al., 2002a); (a) residual velocity and (b) failure time using *RK* and *JC* models. $T_o = 296$ K.

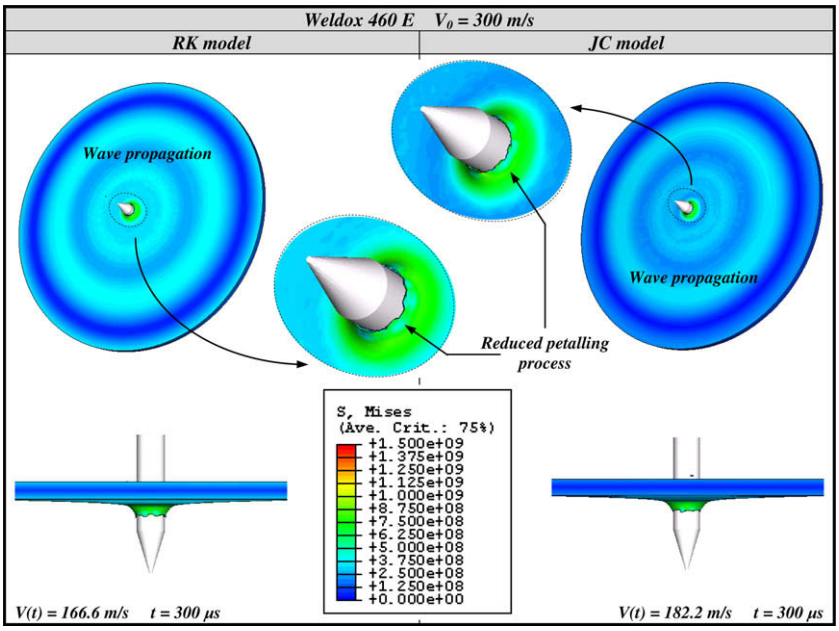

Fig. 30. Equivalent stress contours of the perforation process using *RK* and *JC* models, V_0 = 300 m/s and T_o = 296 K.

7.4. The case of Weldox 460-E steel

In the case of *Weldox 460-E*, numerical simulations of perforation at room temperature have been conducted to estimate the ballistic limit and the residual velocity. The comparison of experimental results with *RK* and *JC* model predictions is shown, Fig. 29. The numerical results obtained using *RK* constitutive relation are the closest to the experiments in terms of residual velocity and failure time. As previously reported in the case of *DH-36* steel, the constitutive relation used to define the behaviour of the target presents a considerable influence in the results obtained using the numerical simulations.

Finally, the results of the numerical simulations in the form of the failure modes are compared after application of *JC* and *RK* models, Fig. 30. It is observed an absence of well developed petalling as reported in Borvik et al. (2002a); Dey et al. (2004). Thus, agreement is found between numerical results and experiments in terms of failure modes.

8. Concluding and remarks

In this paper the thermo-viscoplastic behaviour of *DH-36* and *Weldox 460-E* ferritic steels is examined. Behaviour of *DH-36* steel has been defined using three different constitutive relations, two of them with some physical background (*RK* and *PB*) and another one, purely phenomenological (*JC*). Behaviour of *Weldox 460-E* steel has been defined using *RK* and *JC* models. In the case of *RK* model, the procedure which was used to determine the values of material constants has been outlined. It must be highlighted an excellent agreement found between the analytical predictions obtained by *RK* model and the experimental results used as the reference.

The comparison conducted between the predictions of *RK*, *JC* and *PB* models in a wide range of strain rates and temperatures showed the improved capacity of the *RK* model to define the thermo-viscoplastic behaviour of *DH-36* and *Weldox 460-E* steels.

This demonstrated superiority of *RK* constitutive relation in comparison with *JC* and *PB* formulations is based in the following points:

- The *JC* constitutive relation does not consider the flow stress as decomposed into two parts, the effective stress and the "athermal" stress. Moreover, strain hardening is defined as a power law, without taking into account the effect of strain rate and temperature. The constancy of the strain hardening exponent n in *JC* formulation is contrary to the observations frequently made and reported for metals. The constant logarithmic strain rate sensitivity $\beta = (\partial\bar{\sigma}/\log\dot{\bar{\varepsilon}}_p)_{\bar{\varepsilon}_p,T}$ introduced in the original version of the *JC* model is ineffective to define the strain rate sensitivity of a large number of metals from quasi-static to high strain rates.
- The *PB* constitutive relation is based on the process of thermal activation with an additive decomposition of the total stress. However, it was noticed in this work that the stress decomposition that the model proposes is not in agreement with physical behaviour of materials. For example, the effective stress results dominant during quasi-static loading. Moreover, as it was previously reported in the case of *JC* model, *PB* model does not consider strain hardening exponent as dependant on strain rate and temperature.

Thus, it was possible to conclude the relevance of introducing the strain hardening exponent with dependency on strain rate and temperature in the form: $n = n_0 f(\dot{\bar{\varepsilon}}_p, T)$. This

dependency was included for the first time in constitutive modeling in the *RK* constitutive relation. Using this formulation it is possible to define correctly the thermal softening of the material in adiabatic conditions which causes acceleration of plastic instabilities being precursor of failure. Plastic instabilities frequently take place during impact events due to local high strain rate and temperature levels which are reached during such process.

This was the main reason to apply the *RK* model to *DH-36* and *Weldox-460-E* steel to conduct numerical simulations of impact perforation of plates subjected to high impact velocity by conical projectiles. The numerical results obtained using *RK* model to define the material behaviour are compared with those results obtained using *JC* model.

In the case of *DH-36* steel, different initial temperatures for the target are considered, ($T_{01} = 200$, $T_{02} = 296$, $T_{03} = 400$ K). Relevant differences were found in the ballistic limit, the residual velocity and values of failure time predicted by *RK* and *JC* constitutive relations, especially in the case of higher initial temperature $T_{01} = 200$ K. Thus, it has been noticed the influence of the material definition in the simulation of impact events.

In the case of *Weldox 460-E* steel, the numerical results obtained using *RK* and *JC* models are compared with experimental results. The numerical estimations obtained using the *RK* constitutive relation present a better fitting with experimental results in comparison with the results obtained using the *JC* model.

In further studies, the effects of shear banding, the mechanism reported by Nemat-Nasser and Guo (2003) in *DH-36* steel, should be taken into account in numerical simulations. Certain attempt to describe the contribution of micro-shear banding in plastic flow was presented in Pecherski (1998) and for viscoplastic flow of nanocrystalline materials in Nowak et al. (2007). Moreover, more attention must be also done concerning the failure criterion definition, ultimate stage during the process. In our case a simple failure strain level has been used in agreement with several papers available in the open literature.

Acknowledgements

Janusz Roman Klepaczko passed away on August 15, 2008 at the age of 73. Graduated from Warsaw University of Technology in 1959, began the research work in 1960 at IPPT – Institute of Fundamental Technological Research, Polish Academy of Sciences, Warsaw, Poland and continued it until 1984, becoming full professor in 1983. Since 1985 he was working in LPMM (Laboratory of Physic and Mechanic of Materials), Paul Verlaine University of Metz, France, where he was founder of the experimental laboratory. He was well known in the field of dynamic behaviour of materials; he was the author of over 200 publications and supervised 30 doctors in several research centres around the world. Janusz was involved in research until the end of his life. He was a great researcher and had a passion for Science. He was for us a source of motivation and inspiration.

We pay our tribute to him for his teaching and contribution in Science. The researchers of the University Carlos III of Madrid are indebted to the Comunidad Autónoma de Madrid (Project UC3M/DPI-3395) and to the Ministerio de Educatión y Ciencia de España (Project DPI/2005-06769) for the financial support received which allowed to conduct the numerical simulations of this work.

References

Arias, A., Rodríguez-Martínez, J.A., Rusinek, A., 2008. Numerical simulations of impact behaviour of thin steel to cylindrical, conical and hemispherical non-deformable projectiles. Eng. Frac. Mech. 75, 1635–1656.

Bodner, S.R., Partom, Y., 1975. Constitutive equations for elastic-viscoplastic strain-hardening materials. ASME J. Appl. Mech. 42, 385–389.

Borvik, T., Langseth, M., Hopperstad, O.S., Malo, K.A., 1999. Ballistic penetration of steel plates. Int. Impact. J. Eng. 22, 855–886.

Børvik, T., Hopperstad, O.S., Berstad, T., Langseth, M., 2001. A computational model of viscoplasticity and ductile damage for impact and penetration. Eur. J. Solid Mech. A 20, 685–712.

Borvik, T., Langseth, M., Hoperstad, O.S., Malo, K.A., 2002a. Perforation of 12 mm thick steel plates by 20 mm diameter projectiles with flat, hemispherical and conical noses Part I: Experimental study. Int. J. Impact Eng. 27, 19–35.

Borvik, T., Langseth, M., Hoperstad, O.S., Malo, K.A., 2002b. Perforation of 12 mm thick steel plates by 20 mm diameter projectiles with flat, hemispherical and conical noses Part II: numerical study. Int. J. Impact Eng. 27, 37–64.

Borvik, T., Hopperstad, O.S., Langseth, M., Malo, K.A., 2003. Effect of target thickness in blunt projectile penetration of Weldox 460 E steel plates. Int. J. Impact Eng. 28, 413–464.

Børvik, T., Clausen, A.H., Eriksson, M., Berstad, T., Hopperstad, O.S., Langseth, M., 2005. Experimental and numerical study on the perforation of AA6005-T6 panels. Int. J. Impact Eng. 32, 35–64.

Chocron, I.S., Anderson Jr., C.E., Grosch, D.J., Popelar, C.H., 2001. Impact of the 7.62-mm APM2 projectile against the edge of a metallic target. Int. J. Impact Eng. 25, 423–437.

Chocron, I.S., Anderson Jr., C.E., Behner, T., Hohler, V., 2006. Lateral confinement effects in long-rod penetration of ceramics at hypervelocity. Int. J. Impact Eng. 33, 169–179.

Conrad, H., 1964. Thermally activated deformation in metals. J. Metals 16, 582.

Considère, M., 1885. L'emploi du fer de l'acier dans les constructions. An. Ponts et Chaussées 34, 574–575.

Cowper, G.R., Symonds, P.S., 1952. Strain hardening and strain rate effects in the impact loading of cantilever beams, Brown University, Division of Applied Mechanics, Report No. 28.

Dey, S., Børvik, T., Hopperstad, O.S., Leinum, J.R., Langseth, M., 2004. The effect of target strength on the perforation of steel plates using three different projectile nose shapes. Int. J. Impact Eng. 30, 1005–1038.

Dhulst, Ch.A., Even, D., 2003. Principe d_équivalence temps-température: application de la théorie de l_activation thermique aux aciers. Evolution de la loi plastique avec la vitesse de déformation et la température. Rapport de Maîtrise, Université de Metz avec ARCELOR.

Durrenberger, L., Molinari, A., Rusinek, A., 2007. Internal variable modeling of the high strain-rate behaviour of metals with applications to multiphase steels. Mater. Sci. Eng. A. doi:10.1016/j.msea.2007.06.011.

Fasanella, E.L., Jackson, K.E., Crash simulation of a vertical drop test of a B737 fuselage section with auxiliary fuel tank. US Army Research Laboratory, Vehicle Technology Directorate. NASA (2001) Langley USA.

Forrestal, M.J., Piekutowski, A.J., 2000. Penetration experiments with 6061-T6511aluminum targets and spherical-nose steel projectiles at

striking velocities between 0.5 and 3.0 km/s. Int. J. Impact Eng. 24, 57–67.
Gupta, N.K., Iqbal, M.A., Sekhon, G.S., 2007. Effect of projectile nose shape, impact velocity and target thickness on deformation behaviour of aluminium plates. Int. J. Solids Struct. 44, 3411–3439.
Gupta, N.K., Iqbal, M.A., Sekhon, G.S., 2006. Experimental and numerical studies on the behaviour of thin aluminium plates subjected to impact by blunt – and hemispherical – nosed projectiles. Int. J. Impact Eng. 32, 1921–1944.
Johnson, G.R., Cook, W.H., 1983. A constitutive model and data for metals subjected to large strains, high strain rates and high temperatures. In: Proceedings of Seventh International Symposium on Ballistics, pp. 541–547.
Johnson, G.R., Holmquist, T.J., Anderson Jr., C.E., Nicholls, A.E., 2006. Strain-rate effects for high-strain rate computation. J. Phys. IV France 134, 391–396.
Khan, A., 1998. Continuum Theory of Plasticity. Wiley, New York (Chapter 8).
Klepaczko, J.R., 1965. A power form of the mechanical equation of state with the temperature. Eng. Trans. 13, 561–586.
Klepaczko, J.R., 1975. Thermally activated flow and strain rate history effects for some polycrystalline FCC metals. Mater. Sci. Eng. 18, 121–135.
Klepaczko, J.R., 1987. A practical stress–strain–strain rate-temperature constitutive relation of the power form. J. Mech. Working Technol. 15, 143–165.
Klepaczko, J.R., 1994. An experimental technique for shear testing at high and very high strain rates. The case of a mild steel. Int. J. Impact Eng. 15, 25–39.
Klepaczko, J.R., 1998. A general approach to rate sensitivity and constitutive modeling of FCC and BCC metals. In: Impact: Effects of Fast Transient Loadings, Rotterdam, pp. 3–35.
Klepaczko, J.R., 2005. Review on critical impact velocities in tension and shear. Int. J. Impact Eng. 32, 188–209.
Kobayashi, T., Simons, J.W., Brown, C.S., Shockey, D.A., 2008. Plastic flow behaviour of Inconel 718 under dynamic shear loads. Int. J. Impact Eng. 35, 389–396.
Kocks, U.F., Argon, A.S., Ashby, M.F., 1975. Thermodynamics and kinetics of slip. Progress Mater. Sci. 19, 1–271.
Larour, P., Rusinek, A., Klepaczko, J.R., Bleck, W., 2007. Effects of strain rate and identification of material constants for three automotive steels. J. Steel Res. 78, 348–358.
Liang, R., Khan, A.S., 1999. A critical review of experimental results and constitutive models for BCC and FCC metals over a wide range of strain rates and temperatures. Int. J. Plasticity 15, 963–980.
Martineau, R.L., Prime, M.B., Duffey, T., 2004. Penetration of HSLA-100 steel with tungsten carbide spheres at striking velocities between 08 and 25 km/s. Int. J. Impact Eng. 30, 505–520.
Mae, H., Teng, X., Bai, Y., Wierzbicki, T., 2007. Calibration of ductile fracture properties of a cast aluminum alloy. Mater. Sci. Eng. A 459, 156–166.
Nemat-Nasser, S., 1982. On finite deformation elastoplasticity. Int. J. Solids Struct. 18, 857–872.
Nemat-Nasser, S., Isaacs, J.B., 1997. Direct measurement of isothermal flow stress of metals at elevated temperatures and high strain rates with application to Ta and Ta–W alloys. Acta Mater. 45, 907–919.
Nemat-Nasser, S., Guo, W.G., Liu, M.Q., 1999. Experimentally based micromechanical modeling of dynamic response of molybdenum. Scripta Mater. 40, 859–872.
Nemat-Nasser, S., Guo, W.G., 1999. Flow stress of commercially pure niobium over a broad range of temperatures and strain rates. Mater. Sci. Eng. A 284, 202–210.
Nemat-Nasser, S., Guo, W.G., Kihl, D.P., 2001. Thermochemical response of AL-6XN stainless steel over a wide range of strain rates and temperatures. J. Mech. Phys. Solids 49, 1823–1846.
Nemat-Nasser, S., Guo, W.G., 2003. Thermomechanical response of DH-36 structural steel over a wide range of strain rates and temperatures. Mech. Mat. 35, 1023–1047.
Nowak, Z., Perzyna, P., Pęcherski, R.B., 2007. Description of viscoplastic flow accounting for shear banding. Arch. Metal. Mater. 52, 217–222.
Ono, K., 1968. Temperature dependence of dispersed barrier hardening. J. Appl. Phys. 39, 1803–1806.
Pęcherski, R.B., 1998. Macroscopic effect of micro-shear banding in plasticity of metals. Acta Mech. 131, 203–224.
Piekutowski, A.J., 1999. Holes produced in thin aluminium sheets by the hypervelocity impact of aluminium spheres. Int. J. Impact Eng. 23, 711–722.
Piekutowski, A.J., 2001. Debris clouds produced by the hypervelocity impact of nonspherical projectiles. Int. J. Impact Eng. 26, 613–624.
Rodríguez-Martínez, J.A., Rusinek, A., Zaera, R., Arias, A., Klepaczko, J.R., 2008. Estudio experimental y numérico del comportamiento de láminas de acero sometidas a impacto de media y alta velocidad. Anales de Mecánica de la fractura 25, Madrid, Spain.
Rusinek, A., 2000. Modélisation thermoviscoplastique d'une nuance de tôle d'acier aux grandes vitesses de déformation. Etude expérimentale et numérique du cisaillement, de la traction et de la perforation, Ph.D. Thesis, Université du Metz.
Rusinek, A., Klepaczko, J.R., 2001. Shear testing of sheet steel at wide range of strain rates and a constitutive relation with strain-rate and temperature dependence of the flow stress. Int. J. Plasticity 17, 87–115.
Rusinek, A., Zaera, R., Klepaczko, J.R., Cheriguene, R., 2005. Analysis of inertia and scale effects on dynamic neck formation during tension of sheet steel. Acta Mater. 53, 5387–5400.
Rusinek, A., Zaera, R., Klepaczko, J.R., 2007a. Constitutive relations in 3-D for a wide range of strain rates and temperatures – Application to mild steels. Int. J. Solids Struct. 44, 5611–5634.
Rusinek, A., Zaera, R., 2007b. Finite element simulation of steel ring fragmentation under radial expansion. Int. J. Impact Eng. 34, 799–822.
Rusinek, A., Cheriguene, R., Bäumer, A., Larour, P., 2008a. Dynamic behaviour of high-strength sheet steel in dynamic tension: experimental and numerical analyses. J. Strain Anal. Eng. Des. 43, 37–53.
Rusinek, A., Rodríguez-Martínez, J.A., Arias, A., Klepaczko, J.R., López-Puente, J., 2008b. Influence of conical projectile diameter on perpendicular impact of thin steel plate. Eng. Frac. Mech. 75, 2946–2967.
Rusinek, A., Rodríguez-Martínez, J.A., Zaera, R., Klepaczko, J.R., Arias, A., Sauvelet, C., 2008c. Experimental and numerical analysis on the perforation process of mild steel sheets subjected to perpendicular impact by hemispherical projectiles. Int. J. Impact Eng, doi:10.1016/j.ijimpeng.2008.09.004.
Rusinek, A., Rodríguez-Martínez, J.A., Klepaczko, J.R., Pęcherski, R.B., 2008d. Analysis of thermo-visco-plastic behaviour of six high strength steels. J. Mater. Des.. doi:10.1016/j.matdes.2008.07.034.
Seeger, A., 1957. The mechanism of glide and work-hardening in face-centered cubic and hexagonal close-packed metal. In: Dislocations and Mechanical Properties of Crystals. J. Wiley, New York.
Shanmugama, S., Ramisettia, N.K., Misraa, R.D.K., Hartmannb, J., Janstoc, S.G., in press. Microstructure and high strength–toughness combination of a new 700 MPa Nb-microalloyed pipeline steel. Mater. Sci. Eng. A. doi:10.1016/j.msea.2007.06.003
Simo, J.C., Ortiz, M., 1985. A unified approach to finite deformation elastoplastic analysis based on the use of hyperelastic equations. Comp. Meth. Appl. Mech. Eng. 51, 241–245.
Simo, J.C., Taylor, R.I., 1986. A return mapping algorithm for plane stress elastoplasticity. Int. J. Num. Meth. Eng. 22, 649–670.
Smerd, R., Winkler, S., Salisbury, C., Worswick, M., Lloyd, D., Finn, M., 2005. High strain rate tensile testing of automotive aluminium alloy sheet. Int. J. Impact Eng. 32, 541–560.
Steinberg, D.J., Cochran, S.G., Guinan, M.W., 1980. Constitutive model for metals applicable at high strain rates. J. Appl. Phys. 51 (3), 1498–1504.
Teng, X., Wierzbicki, T., 2006. Evaluation of six fracture models in high velocity perforation. Eng. Fract. Mech. 73, 1653–1678.
Teng, X., Wierzbicki, T., Couque, H., 2007. On the transition from adiabatic shear banding to fracture. Mech. Mater. 39, 107–125.
Teng, X., Wierzbicki, T., Huang, M., 2008. Ballistic resistance of double-layered armor plates. Int. J. Impact. doi:10.1016/j.ijimpeng.2008.01.008.
Voyiadjis, G.Z., Abu Al-Rub, R.K., 2006. A finite strain plastic-damage model for high velocity impacts using combined viscosity and gradient localization limiters: Part II – Numerical aspects and simulations. Int. J. Damage Mech. 15, 335–373.
Voyiadjis, G.Z., Almasri, A.H., 2008. A physically based constitutive model for FCC metals with applications to dynamic hardness. Mech. Mater. 40, 549–563.
Zaera, R., Arias, A., Navarro, C., 2002. Analytical modelling of metallic circular plates subjected to impulsive loads. Int. J. Solids Struct. 39, 659–672.
Zaera, R., Fernández-Sáez, J., 2006. An implicit consistent algorithm for the integration of thermoviscoplastic constitutive equations in adiabatic conditions and finite deformations. Int. J. Solids Struct. 43, 1594–1612.
Zerilli, F.J., Armstrong, R.W., 1987. Dislocation-mechanics-based constitutive relations for material dynamics calculations. J. Appl. Phys. 61, 1816–1825.